AEROMAGNETIC EXPRESSION OF BURIED BASALTIC VOLCANOES NEAR YUCCA MOUNTAIN, NEVADA

By D.W. O'Leary[1], E.A. Mankinen[2], R.J. Blakely[2], V.E. Langenheim[2], and D.A. Ponce[2]

Open-File Report 02-020

Prepared in cooperation with the
U.S. DEPARTMENT OF ENERGY
NEVADA OPERATIONS OFFICE
(Interagency Agreement DE-AI08-96NV11967)

2002

U.S. DEPARTMENT OF THE INTERIOR
U.S. GEOLOGICAL SURVEY

[1]USGS, Denver, Colorado 80225; [2]USGS, Menlo Park, California 94025

TABLE OF CONTENTS

ABSTRACT 1

INTRODUCTION 1

ACKNOWLEDGMENTS 2

PLIO-PLEISTOCENE VOLCANISM NEAR YUCCA MOUNTAIN 2

PREVIOUS AEROMAGNETIC ANOMALY ANALYSIS AND VOLCANIC HAZARDS ASSESSMENT FOR YUCCA MOUNTAIN 4

AEROMAGNETIC DATA AND METHODS OF ANALYSIS 5

POTENTIAL-FIELD MODELING 5

GRAVITY INVERSION 6

MAGNETIC PROPERTIES 6

AEROMAGNETIC ANOMALIES OF CRATER FLAT BASIN 8

AEROMAGNETIC ANOMALIES OF AMARGOSA DESERT 10

PRESENT MODELING RESULTS: PROFILE AA' 12

ANOMALIES I AND G 13

ANOMALY I 14

ANOMALY G 14

PRESENT MODELING RESULTS: PROFILE BB' 15

ANOMALIES L AND M 16

ANOMALIES N AND O 16

DISCUSSION 17

CONCLUSION 19

REFERENCES CITED 21

ILLUSTRATIONS

Figure 1. False color Landsat image showing local geographic features and Plio-Pleistocene volcanic centers near Yucca Mountain 26

2. Ages and locations of basaltic volcanic centers near Yucca Mountain 27

3. Magnetic anomalies, Crater Flat basin, and northern Amargosa Desert, Nevada 28

4. Residual magnetic anomalies, Crater Flat basin, and northern Amargosa Desert, Nevada 29

5. Isostatic residual gravity map of study area 30

6. Depth to basement (pre-Tertiary surface) in the study area 31

7. Magnetic anomalies of possible Plio-Pleistocene basaltic origin 32

8. Residual magnetic anomalies of possible Plio-Pleistocene basaltic origin 33

9. Magnetic anomaly map showing locations of transect AA' and profiles A1 and A2 34

10. Residual magnetic anomaly map showing locations of transect AA' and profiles A1 and A2 35

11. Geophysical model and geologic interpretation of subsurface structure along transect AA' 36

12. Sources for anomalies I and G along transect AA' modeled as buried basaltic bodies 37

13. Source for anomaly I along profile A1 modeled as a buried basaltic body 38

14. Sources for anomalies F and G along profile A2 modeled as buried basaltic bodies 39

15. Magnetic anomaly map showing locations of transect BB' and profile B1 40

16. Residual magnetic anomaly map showing locations of transect BB' and profile B1 41

17. Geophysical model and geologic interpretation of subsurface structure along transect BB' 42

18. Sources for anomalies L and M along transect BB' modeled as buried basaltic bodies 43

19. Source for anomaly M along profile B1 modeled as a buried basaltic body 44

20. Sources for anomalies N and O along transect BB' modeled as buried basaltic bodies 45

21. Aeromagnetic map and superposed Landsat image of outcrops and terrain features of the Yucca Mountain area 46

22. Residual aeromagnetic map and superposed Landsat image of outcrops and terrain features of the Yucca Mountain area 47

TABLE

Table 1. Magnetic anomalies thought to represent buried volcanic centers in the Crater Flat—Amargosa Desert area, Nevada 48

ABSTRACT

A high-resolution aeromagnetic survey has defined a number of small dipolar anomalies indicating the presence of magnetic bodies buried beneath the surface of Crater Flat and the Amargosa Desert. Results of potential-field modeling indicate that isolated, small-volume, highly magnetic bodies embedded within the alluvial deposits of both areas produce the anomalies. Their physical characteristics and the fact that they tend to be aligned along major structural trends provide strong support for the hypothesis that the anomalies reflect buried basaltic volcanic centers. Other, similar anomalies are identified as possible targets for further investigation. High-resolution gravity and ground-magnetic surveys, perhaps along with drilling sources of selected anomalies and radiometric age determinations, can provide valuable constraints in estimating potential volcanic hazard to the potential nuclear waste repository at Yucca Mountain.

INTRODUCTION

Aeromagnetic surveys (U.S. Geological Survey, 1978, 1979; Langenheim and others, 1991) reveal the presence of small dipolar anomalies indicating magnetic bodies buried beneath alluvial deposits of Crater Flat and the northern Amargosa Desert. Some of the anomalies are similar in size and shape to those associated with Pleistocene subaerial basaltic volcanic centers (figure 1) and indicate similar sources buried beneath alluvium. These and other subtle anomalies were more clearly delineated by a high-resolution aeromagnetic survey of the Amargosa Desert collected by the USGS in 1999 (Blakely and others, 2000). This report presents an analysis of magnetic anomalies observed in that survey, interpreted to represent buried basaltic volcanic centers in Crater Flat and in Amargosa Valley near Yucca Mountain.

The geologic record of Plio-Pleistocene volcanism near Yucca Mountain (Crowe and others, 1995) implies that basaltic volcanism could recur within the next million years and perhaps pose a hazard to a potential nuclear waste repository at Yucca Mountain. As part of the Yucca Mountain site characterization program, a probabilistic volcano hazards analysis (PVHA) was carried out (Geomatrix Consultants, 1996). Available information on the locations and ages of Plio-Pleistocene volcanic centers was considered by the PVHA experts and used to characterize the locations, rates, and uncertainties associated with future volcanic activity. The analysis used USGS aeromagnetic survey data (Langenheim and others, 1993) in considering buried volcanic centers. Only one of these suspected buried volcanic centers has been proven by drilling (Carr and others, 1995). The limitations of the PVHA were addressed by Office of

Civilian Radioactive Waste Management (OCRWM) procedure AP-AC.1Q (Expert Elicitation) which states in Section 5.14 (Reassessment) that if new and relevant data become available, the new data need to be assessed to determine their relevance to the assessments of the expert panel. An assessment of the 1999 aeromagnetic survey is presented herein.

This study builds from and references previous modeling and survey efforts. Specific anomalies discussed in the text and shown in the figures are labeled with letters A through T; table 1 cross-references our labels (with the exception of anomaly T which is not a suspected Plio-Pleistocene volcanic center) with those of previous studies. In this study, physical sources of the magnetic anomalies are modeled by bodies having volumes, forms and magnetic susceptibilities comparable to those of the basaltic volcanoes exposed in the vicinity of Yucca Mountain. The modeled bodies are given magnetic properties, geometries, and depths such that the calculated magnetic intensity matches the observed intensity profile. We conducted our analyses at scales of 1:100,000 or larger, although figures in this report are shown at various scales.

ACKNOWLEDGMENTS

We appreciate helpful reviews by T. Hildenbrand and D. Sweetkind, and informal comments by R. Quittmeyer. J. Dohrenwend created the enhanced Landsat images for the USGS. This study was supported by the U.S Department of Energy (DOE) in cooperation with the USGS under Interagency Agreement DE-AI08-96NV11967.

PLIO-PLEISTOCENE VOLCANISM NEAR YUCCA MOUNTAIN

Plio-Pleistocene volcanism near Yucca Mountain is expressed by isolated, relatively small basaltic cinder cones and associated aa lava flows. The volcanoes closest to Yucca Mountain are associated with three events that occurred at about 3.7 Ma, 1.0 Ma and 77 ka (fig. 2). The 3.7-Ma event is characterized by basalt lava flows, exposed dikes, a north-trending alignment of 6-8 vents, and a lack of preserved cones (Connor and others, 2000; p. 424). The 1.0 Ma event is represented by four cinder cones that form a slightly curved NNE alignment in Crater Flat. The youngest volcanic event formed a single cinder cone (Lathrop Wells cone) at the southern extremity of Yucca Mountain.

The eruptive styles and bulk compositions of the basalts are typical of Plio-Pleistocene basalts throughout most of the western Basin and Range province (Hedge and Noble, 1971; Rogers and others, 1995). They probably represent the waning stages of regional crustal volcanism that peaked around 11 Ma. The basalt magmas most likely originated as small,

volatile-rich melt volumes isolated within the upper mantle, possibly a residue of a larger volume formed and mostly erupted around 9-10 Ma. Assuming this general model of melt source (based on petrology and chemistry), the clustering and age of volcanoes in Crater Flat are controlled by local tectonism, not mantle dynamics or subcrustal heat evolution.

Two observations support local tectonic control on volcanism: First, the broadly curvilinear, NNE-trending alignments of volcanoes, notably the 1.0 Ma volcanoes in Crater Flat (fig. 2) and some of the anomalies of inferred Plio-Pleistocene volcanic origin in Amargosa Desert (figs. 3, 4) that conform to the dominant fault strikes at Yucca Mountain, imply that the aligned cones are linked by normal faults. Second, the clustering of exposed volcanoes in Crater Flat basin suggests a causal relationship between the basin and volcano distribution. Crater Flat basin is a depression at least 3 km deep (Langenheim, 2000), bounded on the west by the Bare Mountain fault and less clearly bounded on the east by the Paintbrush Canyon-Stagecoach Road fault (fig. 2). Latitudinally the basin has the structure of a complex half-graben in which the hanging wall (i.e. Yucca Mountain) has subsided across a series of normal faults antithetic to the Bare Mountain fault (Fridrich, 1999; p. 170). Thus, Yucca Mountain extends across the eastern margin of the basin, and part of it has subsided over time into the western reaches of the basin to be buried by alluvium that forms Crater Flat. Because of the alluvium, the structural association of the Plio-Pleistocene basalts and faults of Yucca Mountain is unclear. An isostatic gravity map (fig. 5) shows the shape of the basin and demonstrates that the basin may shallow to the south and have a southern margin corresponding to volcanic outcrops exposed along an eroded ridge north of Highway 95 (figs. 2, 5).

However, the term “local tectonism” should not be interpreted as “exclusively associated with Crater Flat basin.” First, basalts similar to those near Yucca Mountain were erupted in uplifted terrain at Sleeping Butte and Buckboard Mesa at distances of about 39 km and 30 km north from Yucca Mountain, at 350 ka and 2.8 Ma, respectively (Fleck and others, 1996). Second, a relatively large population of suspected buried volcanic centers exists in the Amargosa Desert south of Yucca Mountain. A buried volcanic center in this area (B, table 1 and fig. 3) was confirmed by drilling and yielded an age of approximately 4.0 Ma (Crowe and others, 1995).

If all the suspected buried volcanoes in the Amargosa Desert are about 3.7-4.0 Ma or older, it would imply that the buried volcanic centers form a distinct volcanic field perhaps having its own tectonic controls. Such a volcanic field is likely extinct, judging from the depth of burial. However, if one or more of the suspected buried volcanoes are Pleistocene in age, it would imply existence of a complex tectonic linkage between Amargosa Valley and Crater Flat basin and, locally, a high rate of alluviation in Amargosa Valley relative to Crater Flat.

PREVIOUS AEROMAGNETIC ANOMALY ANALYSIS AND VOLCANIC HAZARDS ASSESSMENT FOR YUCCA MOUNTAIN

Ten PVHA experts were provided data (Langenheim and others, 1993) that showed a buried magnetic body (anomaly A) located 2 km south of Little Cones in Crater Flat and six buried aeromagnetic sources (B-G) in Amargosa Valley south of Yucca Mountain (Table 1, fig. 3). The experts were each asked to define the term “volcanic event” (Geomatrix Consultants, 1996; p. 2-36). They then were asked for their interpretations of the number of volcanic events represented by the aeromagnetic anomalies. (Note that in PVHA a “volcanic event” includes both eruptive and intrusive features: Geomatrix Consultants, 1996; p. 1-1). The number of probable volcanic events represented by the six aeromagnetic anomalies in the Amargosa Desert (Langenheim and others, 1993) ranged from 1 to 12 (Geomatrix Consultants, 1996; p. 3-115), reflecting the experts’ uncertainty in interpreting the anomalies as individual volcanic events. Anomaly B was unanimously counted as a volcanic event because drilling had obtained basalt samples yielding an age of about 4.0 Ma (Crowe and others, 1995). Anomaly D was also accepted, because drilling nearby had obtained basalt fragments (Walker and Eakin, 1963) presumably derived from the anomaly source. Anomalies C and E were considered to delineate individual cones or centers (except by Walker who discounted E). Anomalies F and G were either lumped together as expressing a single volcanic event (McBirney, Walker, Sheridan) or were suspected to represent non-volcanic sources (Walker, Crowe, Carlson).

Based on ground survey data, Connor and others (2000, p. 424) reported a buried magnetic source (C, Table 1; Q, figs. 3, 4) located 2.5 km SW of Northern Cone in Crater Flat (fig. 2). On the basis of the exposed volcanoes, including individual vents (Conner and Hill, 1995; p. 10,116) and anomalies A and Q (Conner and others, 2000), thirteen volcanic events can be counted within Crater Flat (excluding Lathrop Wells cone). The PVHA counted a minimum of two events (at 1.0 Ma and 3.7 Ma) in Crater Flat (Geomatrix Consultants, 1996; p. 3-115).

Ground magnetic surveys in Amargosa Valley reported by Connor and others (1997, 2000) showed that anomalies H, F, and G (Table 1 and figs. 3, 4) comprise three distinct features, interpreted to be basaltic vents, forming a 4.5-km-long, NE-oriented alignment. These individual anomalies form one of several short, northeast-trending alignments suggestive of en echelon structures (Connor and others, 1997, 2000) adjacent to Yucca Mountain.

AEROMAGNETIC DATA AND METHODS OF ANALYSIS

The aeromagnetic data considered in this study (Blakely and others, 2000) cover an area of approximately 2,164 km^2 (836 mi^2), extending from near Beatty, Nevada, east to Little Skull Mountain on the Nevada Test Site (W116°45'-W116°15'45"), and from N36°54'40" south to N36°27'30" (Figs. 3, 4). Aeromagnetic flight lines were oriented east-west, spaced 400 m (0.25 mi) apart, and flown at an altitude of 150 m (500 ft) above terrain, or as low as permitted by safety considerations.

Potential-Field Modeling

Our goal in this study was to determine if aeromagnetic anomalies of the present data set that potentially represent buried volcanoes could be modeled as buried basalt bodies and, using modeling techniques, provide constraints on their shapes and depths of burial. Several target anomalies were selected primarily on the basis of the strong magnetic contrast inferred to exist between volcanic rocks and surrounding alluvium. Models of the magnetic source bodies were constructed with a commercially available 2 1/2-dimensional modeling program ("GM-SYS") based on Webring (1985) that facilitates both forward and inverse calculations. Our models are based on linear profiles across the anomalies and assume that the bodies are two-dimensional in shape but finite in length perpendicular to each profile. In some cases, models are based on multiple profiles in order to constrain the three-dimensional shape of the bodies.

Our models are based primarily on forward calculations, where body shapes are determined by obtaining reasonable fits between observed and calculated profiles via trial-and-error iterations. We also used a direct inverse method (Webring, 1985) to assist the trial-and-error procedure. This method uses non-linear inversion and requires an initial estimate of model parameters (depth, shape, density and susceptibility of suspected sources) and adjusts values of selected parameters in order to reduce the weighted root-mean-square error between observed and calculated gravity and magnetic values. We emphasize that our solutions are not unique because an infinite number of geometric models will have an associated magnetic or gravity field that closely matches the measured field.

No detailed gravity surveys have been conducted in the vicinity of the magnetic anomalies investigated here, and variations in the regional data (Ponce and others, 1999) mainly reflect trends in pre-Tertiary basement (fig. 5). We used the limited gravity values available in the vicinity of our profiles and supplemented those with values extrapolated from the grid in figure 5. The gravity data provide little effect on the modeling process other than to show general trends. The lack of gravity anomalies associated with the magnetic anomalies may indicate that the causative bodies have the same density as the alluvial fill or, in the case of the basaltic

sources, the volumes of the bodies are generally too small to have been detected by the regional-scale gravity surveys (Langenheim, 1995).

Gravity Inversion. As an additional constraint for our models, we used the pre-Tertiary basement surface (fig. 6) derived by Hildenbrand and others (1999). Their estimate of depth to pre-Tertiary basement was based on an inversion of regional gravity data. The inversion procedure, derived by Jachens and Moring (1990), allows the density of basement to vary horizontally as needed, whereas the density of basin-filling deposits is specified by a pre-determined density-depth relationship. The density-depth relationship used by Hildenbrand and others (1999) is based on numerous density data available from the Nevada Test Site (NTS) and vicinity (Mankinen and others, 1999) and is comparable to that determined by Jachens and Moring (1990) for other volcanic basin-fill deposits throughout Nevada. Depths to basement based on well information are used to constrain the calculations. In this iterative approach, a first approximation of the basement gravity field is derived from gravity measurements made on exposed pre-Tertiary rocks, augmented by appropriate basement gravity values calculated at sites where depth to basement is known. This approximation (which ignores the gravity effects of nearby basins) is subtracted from the observed gravity, which provides the first approximation of the basin gravity field. Again using the specified density-depth relation, the thickness of the basin-filling deposits is calculated. The gravitational effect of this first approximation of the basin-filling layer is computed at each known basement station. This effect in turn is subtracted from the first approximation of the basement gravity field and the process is repeated until successive iterations produce no substantial changes in the basement gravity field.

Magnetic Properties. Both paleomagnetic directions and total magnetizations of the rocks in the study area are needed for the interpretation of aeromagnetic anomalies. Pre-Tertiary basement in the area consists chiefly of Precambrian and Paleozoic rocks of varying lithologies. Basement gravity (Hildenbrand and others, 1999) confirms that most of the basement is comprised of carbonate and slightly metamorphosed siliceous sedimentary rocks. Both normal and reversed polarities may be present in such rocks, but their magnetic intensities are generally weak and have little effect on the aeromagnetic field. Dikes, sills and other intrusions associated with the voluminous Tertiary volcanism of the region are likely to be present. Because their densities (~2670 kg/m^3) often are comparable to, or approach, densities of many pre-Tertiary rocks such as Paleozoic and late Precambrian shale and quartzite (Hildenbrand and others, 1999), intrusive rocks may be lumped with pre-Tertiary basement when interpreting the gravity field. Although such intrusive rocks may have

moderate to strong magnetizations, their effect on the aeromagnetic anomalies often is diminished because of depth of burial. Surficial sediments in this region are only weakly magnetic and have negligible effect on aeromagnetic anomalies.

Miocene and younger volcanic rocks of the region are the largest contributors to the aeromagnetic field. The magnetization of a typical volcanic rock has two main components. The *induced component* is proportional to and in the direction of the ambient magnetic field (inclination 62°, declination 15°E at the northern Amargosa Desert). The magnitude of induced magnetization is described by the magnetic susceptibility, the ratio of induced magnetization to ambient magnetic field. The *remanent component*, on the other hand, records the magnetic field of the Earth at the time the volume of rock cooled. The relative importance of induced and remanent components is described by the Koenigsberger ratio, the ratio of remanent to induced component.

When averaged over an appreciable length of time (on the order of 10^4 years), the Earth's magnetic field approximates that of an axial dipole field (inclination 58° to 58.5°, declination 0° over the area shown in fig. 1). The magnetic field has a secular variation, however, causing the actual direction at any given time to vary by as much as 20° from the average direction. Because volcanic rocks erupt and cool over relatively short time periods, their magnetizations are "spot" recordings of the geomagnetic field, and thus could depart from the axial field by as much as 20°. Variations of this magnitude will not significantly affect the models, however, and we therefore use a declination of 0° (180°) and an approximate inclination of +60° (-60°) for rocks possessing normal (reversed) polarity.

Total magnetizations of these rocks (the magnitude of the vector sum of induced and remanent components) are more difficult to characterize than their remanence directions. Magnetizations measured on volcanic rocks from the study area range between 0.1 and 1 A/m (Bath, 1968; Rosenbaum and Snyder, 1985; Ponce and Langenheim, 1995; Grauch and others, 1997, 1999). However, it is not unusual for specific units to have magnetization intensities well outside this range because of variations in composition, grain size, and concentration of magnetic minerals, and because the intensity of magnetization can vary widely within volcanic units, both laterally and vertically (see, for example, Rosenbaum, 1993). The anomalies being investigated are generally isolated, are roughly circular in shape and restricted in areal extent, have high magnetic intensities contrasting with their immediate surroundings, and, thus, are similar to those produced by the basaltic cinder cones and associated flows in Crater Flat (1.1 Ma; Fleck and others, 1996) and at Lathrop Wells (77 ka; Heizler and others, 1999). Small-volume volcanic units, such as the young volcanic cinder cones in this area, cool quickly and thus have high concentrations of small-domain-size magnetite and, consequently, a remanent magnetization typically much stronger than average volcanic rock. The Koenigsberger

ratio of such rocks typically is very high, and induced magnetizations, therefore, contribute little to the overall magnetization. Langenheim (1995), for example, used a remanent magnetization of 10 A/m for models of buried volcanic centers in this area, and Stamatakos and others (1997) used an even higher value (20 A/m) in modeling their ground magnetic survey of Little Cones and surrounding areas in Crater Flat.

AEROMAGNETIC ANOMALIES OF CRATER FLAT BASIN

The aeromagnetic anomaly pattern in Crater Flat basin is dominated by the NNE-striking, fault-induced anomalies of Yucca Mountain, which occupy the eastern half of the basin (figs. 3, 4). The pattern is characterized by chiefly N- and NNE-trending gradients between positive and negative anomalies that mostly reflect down-to-the-west normal fault offsets (Bath and Jahren, 1984; p. 28). The pattern also reflects local contacts between normally magnetized tuffs of the Crater Flat Group and the Topopah Spring Tuff, and the overlying, reversely magnetized Tiva Canyon Tuff (Bath and Jahren, 1985). This fault-dominated anomaly pattern extends westward into Crater Flat, where it is attenuated by burial beneath alluvial deposits. The faulted-tuff anomalies are prominent along the entire southern rim of Crater Flat basin, where the volcanic rocks are exposed along a north-dipping cuesta (fig 1). A prominent E-W magnetic gradient is located at about latitude 36°50' (fig. 3). This gradient probably marks a shallow north-dipping lithologic contact in the Paleozoic basement between carbonates to the south and the strongly magnetic Chainman Shale (formerly mapped as Eleana Formation; Frizzell and Shulters, 1990) to the north (Bath and Jahren 1984, p. 10). Both the Chainman shale and the Eleana Formation are exposed in the Calico Hills (Cole and Cashman, 1999; p. 18; Baldwin and Jahren 1982; p. 26; fig. 1), but the Eleana Formation is allochthonous.

A broad circular positive anomaly about 7 km in diameter and centered at N36°47'18" and W116°32'57" dominates the magnetic field in Crater Flat (fig. 3). Drill hole VH-1 (Carr, 1982; fig. 1) was drilled to investigate the source of this anomaly; the hole encountered 141 m of densely welded, normally magnetized Crater Flat Group tuff before bottoming out at 762 m, still within the tuff. On this evidence, Carr (1982; p. 9) concluded that an unusually thick deposit of Crater Flat Group tuff causes the anomaly. However, modeling of aeromagnetic data shows that an unrealistic thickness of nearly 1000 m of strongly magnetized tuff would be required to produce the anomaly (Langenheim and Ponce, 1995; p. 14). A more likely magnetic source is an igneous body within the pre-Tertiary basement (Langenheim and Ponce, 1995; p. 15). Given the proximity of ~11 Ma basalt, permissive seismic reflections (Brocher and others, 1998), and the requirement for high magnetization of the source, mafic sills are a

likely source for the large positive anomaly in Crater Flat basin (Langenheim and Ponce, 1995).

A large north-south elongated negative anomaly (T; figs 3, 4) occupies the western part of Crater Flat basin. The west side of the anomaly corresponds to the modeled (buried) eastern step of the Bare Mountain fault, which terminates the east-west oriented anomalies of Bare Mountain (Langenheim, 2000; p. 8; fig. 3). Drill hole VH-2, at the east side of this anomaly (Carr and Parrish, 1985; fig. 3), penetrated 30 m of basalt lava flows, breccia, and scoria at a depth of 360 m. The basalt unit lies directly on 11.45-Ma Ammonia Tanks Tuff, has a strong reverse magnetism, and is dated at 11.3 ± 0.1 Ma (Carr and Parrish, 1985; p. 30). Seismic profile data (Brocher and others, 1998) indicate that this unit thickens to the west and pinches out against the Bare Mountain fault. This large negative anomaly most likely represents the extent of the late Miocene basalt (Langenheim, 1995; p. 7; Fridrich, 1999; p. 189), which is interrupted only by anomaly A (Langenheim, 1995; p. 7; fig. 3). The southern extent of the anomaly presumably is represented at the cuesta by outcropping basalt dated 10.5 ± 0.1Ma (Swadley and Carr, 1987; fig. 2).

Anomaly A (figs. 3, 4) culminates at 1.6 km, azimuth 187.65° from Little Cones (figs. 3 and 4). A northwest-oriented, ground magnetic profile extending to pre-Tertiary outcrop in Bare Mountain (Langenheim, 1995; p. 32) shows that anomaly A has two peaks with amplitudes of 200 nT and 800 nT within a distance of about 2 km. The larger peak on the east coincides with a positive gravity anomaly of about 1 mGal (Langenheim, 1995; p. 7). A volcanic source for the main peak of A is suggested by its circularity, a negative dipole effect at its northern side (Connor and others, 1997; p. 75) and its position east of the Bare Mountain fault. Based on ground survey data, Connor and others (1997; p. 75) modeled the source of anomaly A as a thin, roughly circular lava flow at a depth of about 150 m and centered on a buried volcano comparable in volume to the nearby Little Cones (Connor and others, 2000; p. 423).

In order to estimate depth to the source of the main peak of anomaly A, Langenheim (1995) assumed that its source is a narrow, vertically oriented magnetic ribbon (such as a magnetic dike), and related the ground and aeromagnetic field measurements, F_1 and F_2, respectively, to the distances of the source to the height of measurement, r_1 and r_2, using the equation:

$$F_1/F_2 = (r_2/r_1)^2,$$

Where r_2 equals r_1 + 120 m. The amplitude of anomaly A at a height of 120 meters above the ground surface is about 400 nT, and its ground magnetic amplitude is almost 1000 nT. Using the above equation, Langenheim (1995) predicted the depth to the top of the body to be about 206 m. She cautioned, however, that the actual depth to the top of the body would differ from the calculated value if the geometry of the source is radically different than that assumed. Using

Peters' method (Peters, 1949; Blakely, 1995) and assuming that the source is a thin body (Langenheim's (1995) model indicates a thickness of about 100 m) we found that its maximum depth probably is less than 100 m.

A characteristic magnetic anomaly associated with a Plio-Pleistocene basaltic volcano is exemplified by Black cone, one of the exposed 1.0 Ma volcanoes in Crater Flat (figs 1, 2). The sub circular negative anomaly nearly coincides with the area of the volcano and has a distinct positive rim on its north side (figs. 3, 4). Red Cone, also reversely magnetized, produces a more subdued anomaly that is expressed best by the residual magnetic field shown in figure 4. Northern Cone and Little Cones, probably due to their small size, cannot be discerned in figures 3 and 4. In a magnetically "noisy" or generally negatively magnetized terrane, however, even the anomaly produced by Black Cone might be difficult to recognize. This would be particularly true for smaller volcanoes.

Negative anomaly Q, near Northern Cone in Crater Flat (figs. 3, 4), was identified as possibly having a volcanic source (Connor and others, 2000; p. 423). This anomaly does have a peripheral positive peak; if the peak is a dipole effect of volcanic origin the body has been rotated clockwise about 58° (Connor and others, 2000; p. 424). But clockwise rotation of this magnitude for the source of anomaly Q seems unlikely; tectonic rotation at this latitude in Crater Flat basin has been less than 30° (Minor and others, 1997; p. 18), and tectonic rotation associated with extension in post-Miocene time has been negligible (Fridrich and others, 1999; p. 210). The inferred dipole effect may result from faulting in the Yucca Mountain area, or from the large, abrupt changes in magnetic intensity that are known to occur over the tuff layers of Yucca Mountain. These intensity variations attain amplitudes as great as 450 nT (Bath and Jahren, 1985; p. 11, 13). Given the setting and character of the anomalies, it is unlikely that the three negative anomalies, Q, P, and R, represent Plio-Pleistocene volcanic centers. However, figure 4 raises the possibility that these anomalies, along with S, could represent bodies of
10.5-Ma basalt, separated from the larger body (anomaly T) to the south.

AEROMAGNETIC ANOMALIES OF AMARGOSA DESERT

Anomalies B, C, D, F, G and H, in Amargosa Desert (Figs 3, 4) were modeled or discussed by others using ground survey data. The largest of the anomalies (B) covers an area of about 20 km^2. A "dike swarm" model (pinnacles rising above a tabular body) provides a good fit between the observed and calculated magnetic data (Langenheim and others, 1993; p. 1844). The modeled depth to basalt is less than about 150 m (Langenheim and others, 1993; p. 1843). Lack of an associated gravity anomaly indicates a small-volume body within the

alluvium. Langenheim and Ponce (1993) estimated the volume of the source of anomaly B to be 10 to $40x10^7 m^3$. Depth to basement here was estimated at about 800 m based on electrical resistivity data (Greenhaus and Zablocki, 1982). The geophysical model was largely validated by drilling (Carr and others, 1995); Felderhof Federal well 25-1 (figs. 7, 8) encountered basalt (lava breccia or pyroclastic material) at 73 m, reentered alluvium at about 158 m, and penetrated Paleozoic bedrock at 670 m (Carr and others, 1995).

The residual magnetic anomaly B (figs. 4, 8) is complicated, with numerous irregular peaks and depressions that form an irregular anomaly boundary embayed and crenulated by the adjacent normally magnetized field. The anomaly sources are probably an assemblage of overlapping and eroded lava flows cut by dikes and capped by scoria mounds. It probably resembles the exposed, roughly coeval 3.7-Ma basalt center in Crater Flat (fig. 2) from which the original cinder cone edifice(s) has been eroded away. It is likely that a fringe of eroded scoria and basaltic tephra extends beyond the border of anomaly B, as indicated by basalt fragments found in Felderhof Federal well 5-1 (figs. 7, 8) located east of the anomaly border (Carr and others, 1995). The southernmost part of anomaly B features a distinct hook-shaped magnetic low; it may represent a distinct volcanic center within the larger complex. If the linear positive magnetic anomalies extending roughly SW from anomaly B (figs. 7, 8) represent dikes of basalt, they are likely to be ~9.5 Ma and related to basalts exposed farther north at and near Little Skull Mountain (fig. 1).

Anomaly C (figs. 7, 8) was modeled by Langenheim (1995). Because the depth to the top of the source for anomaly C was estimated to be about 200 m and various estimates of depth to basement ranged from about 800 to 1500 m, Langenheim (1995; pp. 9 and 11) concluded that the source body is embedded within the alluvial deposits. An east-west magnetic profile shows two magnetic lows about 1 km apart. Anomaly C is associated with a positive gravity anomaly having an amplitude of about 1 mGal. Anomaly C may represent two cones or vent edifices comparable in thickness to Black or Red Cones in Crater Flat.

Anomaly D (figs. 7, 8) exhibits a double-peaked magnetic high along a south-north profile (Langenheim, 1995; p. 6). The magnetic signature of anomaly D indicates that its source body has a normal magnetic polarity, in contrast to the reversed magnetic polarity indicated for anomaly C. The peaks suggest two vent edifices spaced about 700 m apart (Langenheim, 1995). A 3-mGal gravity high coincides with the location of anomaly D, although here the high may be partly due to topography on the Paleozoic bedrock surface. The thickness of the source body, embedded in alluvium at a depth of about 180 m, is estimated to be about 70 m (Langenheim, 1995).

Present Modeling Results: Profile AA'

In modeling magnetic sources of the area, we first constructed a profile along transect AA' that begins at a point north of Lathrop Wells cone and extends southeast across magnetic anomalies labeled I and G in figures 9 and 10. A suitable model of the exposed cone at Lathrop Wells should lead to better models of similar, concealed cones. In modeling Lathrop Wells cone we used physical properties from the subjacent tuff units that are similar to those used by Mankinen and others (1999) in their models of the Pahute Mesa–Oasis Valley area. In our models, the reversely magnetized Tiva Canyon Tuff is assigned a magnetization of 1 A/m. Older Miocene units are predominately of normal magnetic polarity and are assigned a magnetization of 0.8 A/m. We assigned a magnetization of 10 A/m for the lava flow at Lathrop Wells, which is a conservative estimate for quickly-cooled volcanic units as discussed above, but fairly typical for the area (Langenheim, 1995; Stamatakos and others, 1997). We applied the density/depth distribution of Mankinen and others (1999) to the area containing Miocene volcanic rocks at the northwest end of the profile. We used a density of 1900 kg/m^3 for alluvial fill of the Amargosa Valley and determined that this relatively low value could extend to depths of several hundred meters. The observed gravity (fig. 11B) seems to reflect mainly changes in depth to pre-Tertiary basement.

In our model along AA' (fig. 11C), we show the Lathrop Wells cone directly overlying the reversed polarity Tiva Canyon Tuff. This interpretation is confirmed by an outcrop of Tiva Canyon Tuff at the toe of an aa flow that extends south from the cone (a; figs 9, 10). In this interpretation we find that the magnetic anomaly associated with the Lathrop Wells cone seems to be caused dominantly by the lava flow associated with it.

The high magnetic peak over Lathrop Wells cone (fig. 11A) reflects the combined effect of the 77-ka lava platform and the overlying cinder cone. The lava flow is exposed beyond the southeast flank of the cone. Figures 9 and 10 shows the cinder cone extending about 700 m northwest beyond the anomaly generated primarily by the lava flow. The cinder cone itself apparently contributes little to the magnetic signal as it laps onto the negatively magnetized terrane of the Tiva Canyon Tuff (Swadley and Carr, 1987). This example shows that volcanic centers in this region would not necessarily appear "cone-shaped" in the geophysical model. If, however, there were no associated lava flow, one would still expect the cone itself to be somewhat magnetic because of welding of material along the vent and/or fumaroles, and small, solidified pods of magma probably will be present. In such cases, the modeled source may be more cone-shaped, but the intensity of magnetization probably much weaker.

The falloff of magnetic intensity about 1 km southeast of the Lathrop Wells Cone along transect AA' (fig. 11A) is modeled as a series of normal faults stepping down to the south (fig. 11C). This is one possible interpretation of geologic structure that satisfies the constraints imposed by estimated depths to pre-Tertiary basement and adequately accounts for both observed magnetic (fig. 11A) and gravity data (fig. 11B). Because most of the gravity observations (fig. 11B) were extrapolated from the grid shown in figure 5, a detailed interpretation was not attempted. The geologic interpretation shown in figure 11C is offered as a simple, schematic solution consistent with the geophysical data. The model indicates a thick layer (~250 m) of reversely magnetized Tiva Canyon Tuff overlying the Topopah Spring Tuff and older volcanic rocks. We assigned the same magnetic properties to all the volcanic rocks underlying the Tiva Canyon Tuff and did not attempt to differentiate between them. It should be noted, however, that the apparent thickness of the Tiva Canyon Tuff could be near its maximum value. Rosenbaum and Snyder (1985) showed that the magnetic intensity of Tiva Canyon Tuff exposed at certain localities on Yucca Mountain ranges up to 3 or 4 A/m, values that would decrease the modeled thickness to less than 100 m and more typical of extracaldera accumulations. Unpublished data from Nye County drill holes NC-EWDP-2DB and NC-EWDP-15D (figs. 9, 10) indicate that poorly consolidated Tram Tuff is present at depths ranging from 155 m to 367 m along Highway 95, and that this unit is underlain by as much as 450 m of tuffaceous to calcareous sediment. Approximately 27 m of Topopah Spring Tuff (probably brecciated or disaggregated) were found in NC-EWDP-2DB (figs. 9, 10). Well NC-EWDP-2DB (figs. 9, 10) penetrated Paleozoic carbonate bedrock at about 814 m depth. In general, the recovered borehole cuttings indicate that a significant buried volcanic section exists south of Lathrop Wells and much of it consists of the reversely magnetized Tram Tuff. Taking these observations into account, the overall geological framework can be adjusted in various ways to produce different interpretations of geology and still maintain consistency with the geophysical data. Subsurface data on buried tuff are required to properly adjust the magnetic constraints on the modeled units.

Anomalies I and G. The magnetic field observed along transect AA' over the sources of anomalies I and G is shown in figure 11A. An expanded view of the observed magnetic field and interpretation of geologic structure in the vicinity of anomalies I and G is shown in figure 12. Anomalies I and G are much smaller in amplitude than the anomaly over Lathrop Wells Cone because the sources are buried, and possibly because they are smaller in volume and/or lower in magnetization. We estimated depths to these magnetic sources using Peters' method (Peters, 1949; Blakely, 1995) assuming a thin body. Our calculations indicate that the sources of anomalies I and G occur at about 400 m and 300 m below the magnetometer, respectively. Accounting for the altitude of the aircraft, the tops of the two bodies lie at a maximum depth of

approximately 250 m and 150 m below the topographic surface, respectively. These depths are comparable to those estimated (<300m) for the sources of anomalies C, D, and F (Langenheim, 1995). The amplitudes of the latter aeromagnetic anomalies range from about 300 to 400 nT, whereas anomalies I and G are less than about 50 nT along transect AA'. It is clear that depth of burial is not a sufficient explanation for the low amplitudes of anomalies I and G, and we expect the magnetizations of their causative bodies to be only on the order of 1 to 2 A/m. We used a magnetization of 2 A/m for both. Given these caveats, the modeled bodies (figure 11A) are reasonable approximations of the sources for anomalies I and G. The thickness for the modeled sources of both anomalies I and G is approximately 35 m. Assigning a stronger magnetization to these bodies would decrease their modeled thickness accordingly. The thickness estimated here for the source of anomaly G is a minimum value, however, because transect AA' does not cross its maximum amplitude. Anomaly I shares none of the spatial or magnetic characteristics of anomaly G.

Anomaly I. We modeled anomaly I as a thin basalt body buried by about 250 m of alluvium. The magnetization used for the model (2 A/m) is much stronger than that of the Topopah Spring Tuff, making the tuff an unlikely source for the anomaly unless the body is considerably thicker than the 35 m we estimated above. Figure 13 shows a source model of anomaly I along profile A1 which is approximately perpendicular to transect AA' (figs. 9, 10). Comparing the views of the anomaly I source in figures 13 and 12 indicates an 80-m-thick accumulation (maximum along profile A1) of volcanic material with limited lateral extent. The model suggests that a lava flow extends northeastward from a possible vent area. This flow was modeled using a magnetization of 4 A/m; the apparent thickness, again, will vary depending upon the value chosen for its magnetization.

Anomaly G. Anomaly G has a distinct dipole signature and is reasonably modeled as a basalt body about 150 m below ground surface (fig. 12). We note that the fit between observed and calculated magnetizations above anomaly G could be improved if we rotated the magnetization direction away from the nominal values used (I=-60°, D=180°). The ground magnetic survey of anomaly G shows conspicuous NE-trending linear characteristics (Connor et al., 1997; p 75) and may be part of an aligned group of volcanic centers (anomalies H, F, G, figs. 7, 8; Connor and others, 2000; p. 424).

Figure 14 shows one subsurface geologic interpretation along profile A2, which crosses transect AA' obliquely (figs. 9, 10). Profile A2 was oriented as close to north-south as possible while still crossing the maximum amplitudes of anomalies F and G. Few gravity observations are available along this profile, and thus only the magnetic data are modeled here. Peters' method (Peters, 1949; Blakely, 1995) indicates maximum depths of approximately 250 m and 150 m to the sources of anomalies F and G, respectively. A magnetization of 2 A/m

was used for both bodies. The observed magnetization along this profile proved more difficult to match than others described in this report. The mismatch at the south end of the profile, however, obviously is due in part to the influence of anomaly H and other, more subtle anomalies in this area (fig. 3). Although the relative shapes of the anomalies can be matched, considerable discrepancy remains (fig. 14A). One possible explanation for the mismatch could be a considerable difference in remanent magnetization direction between the two bodies, as demonstrated in figure 14B. In this hypothetical example, the bodies causing anomalies F and G are given inclinations of -40° and -70°, respectively, which are within permissible limits based on modern geomagnetic secular variation. The maximum thickness along profile A2 for the modeled sources of anomalies F and G is approximately 70 m and 40 m, respectively.

Profile BB'

The group of positive anomalies, L, M, N, and O crossed by transect BB' (figs. 15, 16), is difficult to interpret. Figure 17 shows an interpretation of these anomalies assuming that they reflect volcanic bodies. Various attempts at modeling the magnetic field in this area seem to indicate that the sources for anomalies L through O probably are not isolated bodies totally surrounded by non-magnetic alluvium. The models seem most geologically reasonable if there is a widespread, older magnetic unit underlying the smaller bodies and providing the continuity of magnetic character that seems apparent over much of this part of the study area (figs. 3, 15). Our preferred interpretation is that there is a normal-polarity volcanic unit (Miocene tuff?) overlying older, non-magnetic or weakly magnetic strata in the Amargosa Desert. The causative bodies for anomalies L, M, N, and O are modeled as lying on this inferred Miocene tuff. Using Peters' method and assuming a thin body, we estimate that the bodies producing anomalies L and M, and are approximately 300 m below the magnetometer, those producing anomaly N and O at about 450 m and 350 m, respectively. Again correcting for the altitude of the aircraft, the tops of the bodies should range from about 250m below the topographic surface beneath anomaly N to perhaps as shallow as 50 m beneath anomaly O.

Figure 17A indicates that the maximum amplitude of anomalies L, M, N, and O (at 150 m above the ground surface) is roughly 70 nT, compared to nearly 400 nT for anomaly A located approximately 5 km north of anomaly O (figs. 3, 4). This indicates that the causative bodies along profile BB' must have a much weaker magnetization and/or be located deeper than that producing anomaly A. Because the sources of anomalies A, L, M, N, and O all lie at comparable depths, the magnetizations of the sources for anomalies O to L must be weaker than anomaly A. We use 3 A/m for our model bodies.

Figure 17C shows a tentative geologic interpretation that satisfies the constraints imposed by estimated depths to pre-Tertiary basement and based on the gravity data (figs. 6, 17B). Only an approximate match to the few available gravity observations was attempted, using the density/depth distribution of Mankinen and others (1999). The trends in observed gravity again mainly reflect changes in depth to pre-Tertiary basement. The interpretation shown in figure 17C uses the lithology encountered in Crater Flat drill hole VH-1 (Carr, 1982) as a guide. At that locality, approximately 155 m of basalt, basaltic cinders, and alluvium overlies a 106-m-thick layer of Tiva Canyon Tuff. The top of an underlying 294-m-thick layer of Topopah Spring Tuff is at a sufficiently high level that it could have overflowed the margin of the Crater Flat basin onto earlier non-magnetic or weakly magnetic fill of the Amargosa Desert. This interpretation does not preclude the possibility that a younger, normally magnetized Miocene tuff, such as the Ammonia Tanks Tuff, is the unit that underlies this part of the Amargosa Desert. Our model in the vicinity of anomalies L through O, however, would remain the same in either case. Although this interpretation is admittedly simplistic, it is designed to demonstrate the possible influence of additional volcanic source bodies on the magnetic profile.

Anomalies L and M. Our interpretation of geologic structure in the vicinity of anomalies L and M is shown in figure 18. Also shown in figure 18 is the location of profile B1, which is perpendicular to profile BB' at anomaly M (figs. 15, 16). The source bodies for anomaly L and M were modeled using a magnetization of 3 A/m, and observed and calculated magnetic fields
(fig. 18) are in good agreement. The two bodies appear to overlap in part. The maximum thickness for the modeled sources of anomalies L and M is approximately 40 m and 50 m, respectively. Figure 19 shows a section through the modeled source of anomaly M along profile B1. Comparing the views of the anomaly M source in figures 18 and 19 indicates a thin, somewhat broad layer of volcanic material that has the appearance of a flow rather than the thicker, more localized accumulation indicated by our modeling of anomaly I.

Anomalies N and O. Our interpretation of geologic structure in the vicinity of anomalies N and O is shown in figure 20. The related sources for anomaly N and O were modeled using a magnetization of 3 A/m, and observed and calculated magnetic fields (figs. 20, 17A) again are in good agreement. Although the depths to the two sources differ, the modeled bodies appear very similar to those producing anomalies L and M. The maximum thickness for the modeled sources of anomalies N and O is approximately 30 m and 20 m, respectively.

The irregular shapes of the anomalies (L is circular, M and N are crescent shaped, O is lozenge shaped) and their association with the inferred Carrara fault and perhaps with older basalt bodies (e.g., anomaly "b" of Connor and others, 2000, p. 423; figs. 15, 16), raise the possibility that the source bodies could be basalt of late Miocene age. It seems less likely, however, that the sources are faulted Miocene tuffs because the intrinsic magnetization of those siliceous units likely would be much weaker and the bodies consequently much larger than indicated in our model. Small outcrops in the vicinity of BB' give conflicting information. The outcrop of normally magnetized Ammonia Tanks Tuff ("t", figs. 15, 16; Swadley and Carr, 1987) occurs within a larger negative anomaly possibly produced by reversely magnetized basalt, or the Tiva Canyon or Rainier Mesa Tuffs (Langenheim and Ponce, 1995; p. 14), indicating that the outcrop must be part of a relatively small block. Likewise, outcrops of Zabriskie Quartzite
("z", figs. 15, 16; Swadley and Carr, 1987) are in an area where the gravity inversion indicates basement to be no shallower than about 350 m (fig. 6) and they may thus be allochthonous. No gravity data are available in or near the Zabriskie Quartzite outcrops (fig. 5) and new gravity observations are needed to help resolve this problem.

DISCUSSION

We believe that our models are reasonable approximations of the causative bodies producing the small magnetic anomalies in the Crater Flat and northern Amargosa Desert area. The intensities of magnetization in our models are weaker than those measured at exposed volcanic centers in Crater Flat and those used in previous modeling studies (Langenheim, 1995; Connor and others, 2000). However, the anomalies themselves are weaker and were not well delineated until recognized in the high-resolution aeromagnetic data (Blakely and others, 2000), indicating either that the sources are small in volume, low in magnetization, or a combination of both. On the other hand, the magnetizations we use (1 to 4 A/m) are entirely consistent with strongly magnetized volcanic rock.

Two important inferences can be drawn from our models: (1) The shape and lateral extent of the bodies are consistent with buried volcanic centers, and (2) the volume of volcanic material is small. We estimate that the source of anomaly M, for example, has a volume of roughly 0.5×10^7 m^3. This estimate is less than the range reported for the sources of anomalies B, C, D and E by Langenheim and Ponce (1993; 1 to 40×10^7 m^3) but are within the order of magnitude estimate of error. The volume could be greater if relatively nonmagnetic material also is present, as is the case at the Lathrop Wells Cone, where cinder comprises much of the cone. Although the lateral shapes of our modeled bodies are probably reasonable, their

thickness will vary depending on the intensity of magnetization used. Nevertheless, none of the volumes will be grossly different, and all of our modeled bodies clearly fit into any classification of a small-volume volcanic field (see, for example, Crowe, 1986). Most likely, the basalt centers were scoured by erosion in the process of burial, and little, if any, cone structures remain. Inferred rates of alluviation imply that buried volcanic centers are of pre-Pleistocene age (Langenheim, 1995).

It is interesting to note that depths to most of the sources are roughly the same, suggesting that the volcanic centers were erupted onto a common paleosurface within the alluvial fill. In the immediate vicinity of anomalies O, N, M, and L, part of that paleosurface may include the eroded surface of a widespread Miocene tuff. The paleosurface must have been ancient prior to eruptions of the volcanic centers because both normal- and reversed-polarity sources overlie it. Reversed polarity rocks probably erupted during the Matuyama Reversed Polarity Chron, which lasted from 2.59 to 0.78 Ma (see, for example, Baksi, 1995), but eruption during an earlier period of reversed magnetic polarity is not precluded. Similarly, the normal polarity rocks could date from the Brunhes Normal Polarity Chron (780 ka to present), possibly one of the longer subchrons (Jaramillo or Olduvai) of the Matuyama Chron, or any of the post-middle Miocene periods of normal magnetic polarity.

Groups of closely spaced vents/volcanic centers in the area may be localized along faults (Connor and others, 2000). Anomalies O, N, M, and L are particularly interesting in this respect because they are approximately parallel to the Crater Flat alignment of Connor and others (2000). A fault, 5 km or more in length, may have provided access through the Topopah Spring Tuff. Connor and others (2000) also pointed out the “AAA alignment” through anomalies H, F, and G. Vents that cluster in close proximity often have the same paleomagnetic direction, suggesting that they erupted in a single volcanic episode. The 1.0 Ma volcanic centers in Crater Flat, for example, all share the same paleomagnetic direction (Champion, 1995), suggesting that little time elapsed between eruptions. Above, we speculate that the sources for anomalies F and G, although both reversely magnetized, may have significantly different remanent magnetization directions. If true, these bodies must have erupted at times separated by some tens, if not hundreds, of years based on normal rates of geomagnetic secular variation (see, for example, Hagstrum and Champion, 1995, 2001). Such small time intervals are unlikely to be resolved with radiometric techniques. Although part of the same volcanic episode, the eruptions need not have been simultaneous.

We find no convincing evidence for buried basaltic vents in Jackass Flats (fig. 1). Jackass Flats is dominated by short west-northwest-trending gradients and longer but uneven northeast trending gradients (fig. 22). The WNW-trending gradient may represent down to the south normal faults. The most conspicuous feature is the broad positive anomaly that extends

NNE into Jackass Flats from anomaly B (figs. 21, 22). The intensity and the “rough” surface of this positive anomaly suggest basalt layers on the hanging wall of the gravity fault. The basalt flow(s) would be of the 9.5 Ma series that caps Little Skull Mountain and crops out within positive anomalies elsewhere in Jackass Flats. No source vents have been found for these basalts, but flows probably moved southward from central Jackass Flats along the gravity fault.

CONCLUSION

Our primary goal was to determine if newly delineated, but subtle, aeromagnetic anomalies in the current data set could be modeled as buried basaltic volcanoes. The seven anomalies we chose to investigate were successfully modeled as basaltic bodies. Other interpretations of the anomalies are possible but investigation of alternative models is beyond the scope of the present study. It should be emphasized, however, that because of the strong magnetizations required to produce the suspect anomalies, their source bodies are most likely volcanic in origin. Some anomalies have a high probability of being caused by Plio-Pleistocene basaltic volcanoes/cinder cones such as the Lathrop Wells cone and the 1.0 Ma Crater Flat vents. Others anomalies may eventually prove to reflect relatively shallow occurrences of Miocene tuff, albeit the source bodies in those cases must be significantly larger than modeled here because the strength of magnetization of those siliceous units is less than that of the basaltic cones/vents.

Based on the results of our modeling and additional examination of the 1999 USGS aeromagnetic data, sources for several other magnetic anomalies in the Amargosa Desert seem likely candidates to be of basaltic volcano origin. We assign tentative rankings to the anomalies reflecting our degree of confidence that they in fact express buried basaltic volcanoes/vents; the rank numbers shown in Table 1 are keyed to qualitative terms that express our belief that a given anomaly has a volcanic source. As described earlier, only one of the buried sources (for anomaly B) has been drilled and sampled; it is therefore a confirmed volcanic source (“conf.”, Table 1). Anomaly B is much larger than any of the others on the aeromagnetic map (fig. 3) and the character of the residual magnetic field (fig. 4) indicates that the center may consist of a number of clustered or nested vents.

A high degree of confidence is assigned to those anomalies exhibiting a pronounced dipole signature, i.e., a subcircular positive (negative) anomaly with a distinct negative (positive) rim. Candidates among this group are anomalies A, C, D, F, G, and H (Table 1, figs. 3, 4). Anomaly D is ranked highest among these because of basalt fragments encountered in nearby drilling (Walker and Eakin, 1963).

We are less confident about anomalies E, I, L, M, N, and O (Table 1, figs. 3, 4) because they lack definitive dipole signatures. The subcircular shape of the anomalies, however, is highly suggestive as is the apparently strong magnetization of the source bodies. Anomalies L, M, N, and O also are approximately parallel to the Crater Flat and H-to-G alignments possibly indicating structural control of volcanic eruptions. Anomaly E has a relatively high rank (Table 1, figs. 3, 4) because of its circular shape.

Anomalies J and K may have deeply buried volcanic sources, and their alignment with anomaly E suggests a volcanic vent alignment, but anomalies J and K may have less significance in the evaluation of volcanic hazards because the source bodies appear to be more deeply buried and thus could be significantly older than the other basalts. The association of anomaly J with an irregular, northwest oriented cluster of positive anomalies (figs 3, 4) suggests that it could also be a basement feature rather than a separate volcanic vent/edifice.

Models derived from potential-field data are not unique. In a mathematical sense, an infinite variety of models satisfy any given magnetic anomaly, and additional studies may aid in determining which model is most geologically reasonable. Several investigations would test and constrain our models of volcanic bodies beneath Crater Flat and the northern Amargosa Desert. Detailed ground or helicopter magnetic surveys over specific anomalies would enhance details of the magnetic properties and geometries of the volcanic centers. High-resolution gravity and seismic-reflection surveys might detect low-density, low-velocity volcanic material at depth. A final test might entail drilling into one or more of the proposed volcanoes. Obtaining basalt samples and radiometric ages from the samples would aid in refining the calculation of recurrence and in determining whether a distinct population of older ($\geq$ 3.7 Ma) volcanoes exists beneath the Amargosa Desert.

References cited

Baksi, A.K., 1995, Fine tuning the radiometrically derived geomagnetic polarity time scale (GPTS) for 0-10 Ma: Geophysical Research Letters, v. 22, p. 457-460.

Baldwin, M. J. and Jahren, C. E., 1982, Magnetic properties of drill core and surface samples from the Calico Hills area, Nye County, Nevada; U.S. Geological survey Open-File Report 82-536, 27 p.

Bath, G.D., 1968, Aeromagnetic anomalies related to remanent magnetism in volcanic rock, Nevada Test Site, *in* Eckel, E.B., editor, Nevada Test Site: Geological Society of America Memoir 110, p. 135-156.

Bath, G. D. and Jahren, C. E., 1984, Interpretations of magnetic anomalies at a potential repository site located in the Yucca Mountain area, Nevada Test Site; U. S. Geological Survey Open-File Report 84-120, 40 p.

Bath, G. D. and Jahren, C. E., 1985, Investigation of an aeromagnetic anomaly on west side of Yucca Mountain, Nye County, Nevada: U.S. Geological Survey Open-File Report 85-459, 24 p.

Blakely, R.J., 1995, *Potential Theory in Gravity and Magnetic Applications*: Cambridge University Press, 441 p.

Blakely, R.J., Langenheim, V.E., Ponce, D.A., and Dixon, G.L., 2000, Aeromagnetic survey of the Amargosa Desert, Nevada and California: A tool for understanding near-surface geology and hydrology: U.S. Geological Survey Open-File Report 00-188, 35 p.

Brocher, T. M., Hunter, W. C. and Langenheim, V. E., 1998, Implications of seismic reflection and potential field geophysical data on the structural framework of the Yucca Mountain-Crater Flat region, Nevada: Geological Society of America Bulletin, v. 110, p. 947-971.

Carr, W.J., 1982, Volcano-tectonic history of Crater Flat, southwestern Nevada, as suggested by new evidence from drill hole USW-VH-1 and vicinity: U.S. Geological Survey Open-File Report 82-457, 23 p.

Carr, W. J., 1984, Regional structural setting of Yucca Mountain, southwestern Nevada, and late Cenozoic rates of tectonic activity in part of the Southwestern Great Basin, Nevada and California: U. S. Geological Survey Open File Report 84-854, 109 p.

Carr, W. J. and Parrish, L. D., 1985, Geology of drill hole USW-VH-2, and structure of Crater Flat, southwestern Nevada: U. S. Geological Survey Open File Report 85-475, 41 p.

Carr, W. J., Grow, J. A. and Keller, S. M., 1995, Lithologic and geophysical logs of drill holes Felderhoff Federal 5-1 and 25-1, Amargosa Desert, Nye County, Nevada: U.S. Geological Survey Open-File Report 95-155, 14 p.

Champion, D.E., 1995, Volcanic episodes near Yucca Mountain as determined by paleomagnetic studies at Lathrop Wells, Crater Flat, and Sleeping Butte, Nevada: U.S. Geological Survey Open-File Report 95-563, 9 p.

Connor, C. B., and Hill, B.E., 1995, Three nonhomogeneous Poisson models for the probability of basaltic volcanism: Applications to the Yucca Mountain region, Nevada: Journal of Geophysical Research, v. 100, p. 10,107-10,125.

Connor, C. B., Lane-Magsina, S., Stamatakos, J. A., Martin, R. H., LaFemina, P. C., Hill, B. E. and Lieber, S., 1997, Magnetic surveys help reassess volcanic hazards at Yucca Mountain, Nevada: Eos, Transactions of the American Geophysical Union; v. 78, no. 7, p. 73-76.

Connor, C.B., Stamatakos, J.A., Ferrill, D.A., Hill, B.E., Ofoegbu, G.I., Conway, F.M., Sagar, B., and Trapp, J., 2000, Geologic factors controlling patterns of small-volume basaltic volcanism: Application to a volcanic hazards assessment at Yucca Mountain, Nevada: Journal of Geophysical Research, v. 105, p. 417-432.

Crowe, B.M., 1986, Volcanic hazard assessment for disposal of high-level radioactive waste, (Chap. 16) *in* Active Tectonics: Impact on Society: National Academy Press, Washington, D.C., p. 247-260.

Crowe, B., Perry, F., Geissman, J., McFadden, L., Wells, S., Murrell, M., Poths, J., Valentine, G. A., Bowker, L. and Finnegan, K., 1995, Status of volcanism studies for the Yucca Mountain Site Characterization Project, Los Alamos National Laboratory, LA-12908-MS.

Fleck, R.J., Turrin, B.D., Sawyer, D.A., Warren, R.G., Champion, D.E., Hudson, M.R., and Minor, S.A., 1996, Age and character of basaltic rocks of the Yucca Mountain region, southern Nevada: Journal of Geophysical Research, v. 101, p. 8205-8227.

Fridrich, C.J., 1999, Tectonic evolution of the Crater Flat basin, Yucca Mountain region, Nevada, *in* Wright, L. A., and Troxel, B. W., editors, Cenozoic Basins of the Death Valley Region: Geological Society of America Special Paper 333, Boulder, Colorado, Geological Society of America, p. 169-195.

Fridrich, C. J., Whitney, J. W. and Hudson, M. R., 1999, Space-time patterns of late Cenozoic extension, vertical axis rotation, and volcanism in the Crater Flat basin, southwest Nevada, *in* Wright, L.A. and Troxel, B. W., editors, Cenozoic Basins of the Death Valley Region: Geological Society of America Special Paper 333, Geological Society of America, Boulder, Colorado, p.197-212.

Frizzell, V.A., Jr., and Shulters, J., 1990, Geologic map of the Nevada Test Site, southern Nevada: U.S. Geological Survey Miscellaneous Investigations Map I-2046, scale 1:100,000.

Geomatrix Consultants, 1996, Probabilistic volcanic hazard analysis for Yucca Mountain, Nevada. No. BA0000000-01717-2200-00082, Rev. 0; San Francisco, CA.

Grauch, V.J.S., Sawyer, D.A., Fridrich, C.J., and Hudson, M.R., 1997, Geophysical interpretations west of and within the northwestern part of the Nevada Test Site: U.S. Geological Survey Open-File Report 97-476, 45 p.

Grauch, V.J.S., Sawyer, D.A., Fridrich, C.J., and Hudson, M.R., 1999, Geophysical framework of the southwestern Nevada volcanic field and hydrologic implications: U.S. Geological Survey Professional Paper.1608, 39 p.

Greenhaus, M.R., and Zablocki, C.J., 1982, A Schlumberger resistivity survey of the Amargosa Desert, southern Nevada: U.S. Geological Survey Open-File Report 82-897, 150 p.

Hagstrum, J.T., and Champion, D.E., 1995, Late Quaternary geomagnetic secular variation from historical and ^{14}C-dated lava flows on Hawaii: Journal of Geophysical Research, v. 100, p. 24,393-24,403.

Hagstrum, J.T., and Champion, D.E., 2001, A Holocene paleosecular variation record from ^{14}C-dated volcanic rocks in western North America: Journal of Geophysical Research, in press.

Hedge, C. E., and Noble, D. C., 1971, Upper Cenozoic basalts with high Sr^{87}/Sr^{86} and Sr/Rb ratios, southern Great Basin, western United States: Geological Society of America Bulletin, v. 82, p. 3503-3510.

Heizler, M.T., Perry, F.V., Crowe, B.M., Peters, L., and Appelt, R., 1999, The age of Lathrop Wells volcanic center: An $^{40}Ar/^{39}Ar$ dating investigation: Journal of Geophysical Research,
v. 104, p. 767-804.

Hildenbrand, T.G., Langenheim, V.E., Mankinen, E.A., and McKee, E.H., 1999, Inversion of gravity data to define the pre-Tertiary surface and regional structures possibly influencing ground-water flow in the Pahute Mesa-Oasis Valley region, Nye County, Nevada: U.S. Geological Survey Open-File Report 99-49, 26 p.

Jachens, R.C., and Moring, B.C., 1990, Maps of the thickness of Cenozoic deposits and the isostatic residual gravity over basement for Nevada: U.S. Geological Survey Open-File Report 90-404, 15 p.

Langenheim, V.E., 1995, Magnetic and gravity studies of buried volcanic centers in the Amargosa Desert and Crater Flat, southwest Nevada: U.S. Geological Survey Open-File Report 95-564, 37 p.

Langenheim, V.E., 2000, Constraints on the structure of Crater Flat, southwest Nevada, derived from gravity and magnetic data; *in* Whitney, J.W., and Keefer, W.R., editors, Geologic and

geophysical characterization studies of Yucca Mountain, Nevada, a potential high-level radioactive-waste repository: U.S. Geological Survey Digital Data Series 058, 11p.

Langenheim, V.E., Carle, S.F., Ponce, D.A., and Phillips, J.D., 1991, Revision of an aeromagnetic survey of Lathrop Wells area, Nevada: U.S. Geological Survey Open-File Report 91-46,
12 p., 1 magnetic tape.

Langenheim, V.E., Kirchoff-Stein, K.S., and Oliver, H.W., 1993, Geophysical investigations of buried volcanic centers near Yucca Mountain, southwest Nevada: Proceedings, Fourth International Conference, High Level Radioactive Waste Management, Las Vegas, Nevada, v. 2, p. 1840-1846.

Langenheim, V.E., and Ponce, D. A., 1993, Volume of buried volcanic centers near Yucca Mountain, southwest Nevada, as calculated from aeromagnetic data: Eos, Transactions of the American Geophysical Union, v. 74, no. 43, p. 222.

Langenheim V.E., and Ponce, D.A., 1995, Ground magnetic studies along a regional seismic-reflection profile across Bare Mountain, Crater Flat and Yucca Mountain, Nevada: U.S. Geological Survey Open-File Report 95-834, 36 p.

Mankinen, E.A., Hildenbrand, T.G., Dixon, G.L., McKee, E.H., Fridrich, C.J., and Laczniak, R.J., 1999, Gravity and magnetic study of the Pahute Mesa and Oasis Valley region, Nye County, Nevada: U.S. Geological Survey Open-File Report 99-303, 57 p.

Minor, S.A., Hudson, M.R. and Fridrich, C.J., 1997, Fault-slip data, paleomagnetic data, and paleostress analyses bearing on the Neogene tectonic evolution of northern Crater Flat basin, Nevada: U.S. Geological Survey Open File Report 97-285, 41 p.

Monsen, S.A., Carr, M.D., Reheis, M.C. and Orkild, P.P., 1992, Geologic map of Bare Mountain, Nye County, Nevada: U. S. Geological Survey Miscellaneous Investigations Series Map I-2201, scale 1:24,000.

Peters, L.J., 1949, The direct approach to magnetic interpretation and its practical application: Geophysics, v. 14, p. 290-320.

Ponce, D.A., and Langenheim, V.E., 1995, Gravity and magnetic investigations of the Ghost Dance and Solitario faults, Yucca Mountain, Nevada: U.S. Geological Survey Open-File Report 95-521, 26 p.

Ponce, D.A., Mankinen, E.A., Davidson, J.G., Morin, R.L., and Blakely, R.J., 1999, Digital isostatic gravity map of the Nevada Test Site and vicinity, Nye, Lincoln, and Clark Counties, Nevada, and Inyo County, California: U.S. Geological Survey Open-File Report 99-554-C, scale 1:120,000.

Rogers, N. W., Hawkesworth, C. J., and Ormerod, D. S., 1995, Late Cenozoic basaltic volcanism in the western Great Basin, California and Nevada: Journal of Geophysical Research, v. 100, p. 10,287-10,301.

Rosenbaum, J.G., 1993, Magnetic grain-size variations through an ash flow sheet: Influence on magnetic properties and implications for cooling history: Journal of Geophysical Research, v. 98, p. 11,715-11,727.

Rosenbaum, J.G., and Snyder, D.B., 1985, Preliminary interpretation of paleomagnetic and magnetic property data from drill holes USW G-1, G-2, GU-3, G-3, and VH-1 and surface localities in the vicinity of Yucca Mountain, Nye County, Nevada: U.S. Geological Survey Open-File Report 85-49, 73 p.

Sawyer, D.A., Fleck, R.J., Lanphere, M.A., Warren, R.G., Broxton, D.E., and Hudson, M.R., 1994, Episodic caldera volcanism in the Miocene southwestern Nevada volcanic field: Revised stratigraphic framework, $^{40}Ar/^{39}Ar$ geochronology, and implications for magmatism and extension: Geological Society of America Bulletin, v. 106, p. 1304-1318.

Stamatakos, J.A., Connor, C.B., and Martin, R.H., 1997, Quaternary basin evolution and basaltic volcanism of Crater Flat, Nevada, from detailed ground magnetic surveys of the Little Cones: Journal of Geology, v. 105, p. 319-330.

Swadley, W C and Carr, W. J., 1987, Geologic map of the Quaternary and Tertiary deposits of the Big Dune Quadrangle, Nye County, Nevada, and Inyo County, California: U. S. Geological Survey Miscellaneous Investigations Series Map I-1767, scale 1:24,000.

U.S. Geological Survey, 1978, Aeromagnetic map of Lathrop Wells area, Nevada: U.S. Geological Survey Open-File Report 78-1103, 3 sheets, scale 1:62,500.

U.S. Geological Survey, 1979, Aeromagnetic map of the Timber Mountain area, Nevada: U.S. Geological Survey Open-File Report 79-587, scale 1:62,500.

Walker, G.E., and Eakin, T.E., 1963, Geology and ground water of Amargosa Desert, Nevada-California: State of Nevada Department of Conservation and Natural Resources Reconnaissance Series Report 14, 45 p.

Webring, M., 1985, SAKI-FORTRAN program for generalized linear inversion of gravity and magnetic profiles: U.S. Geological Survey Open-File Report 85-122, 29 p.

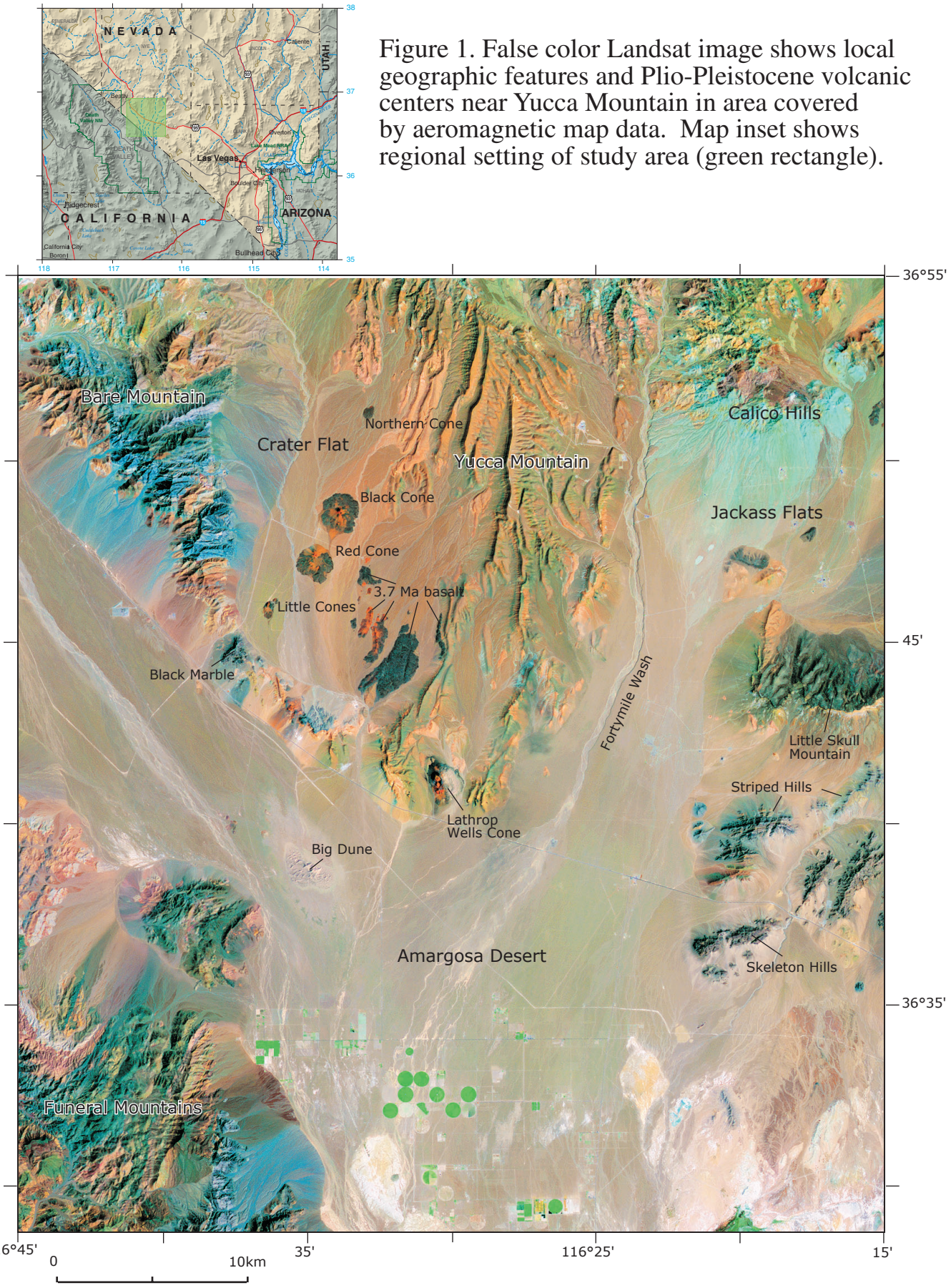

Figure 1. False color Landsat image shows local geographic features and Plio-Pleistocene volcanic centers near Yucca Mountain in area covered by aeromagnetic map data. Map inset shows regional setting of study area (green rectangle).

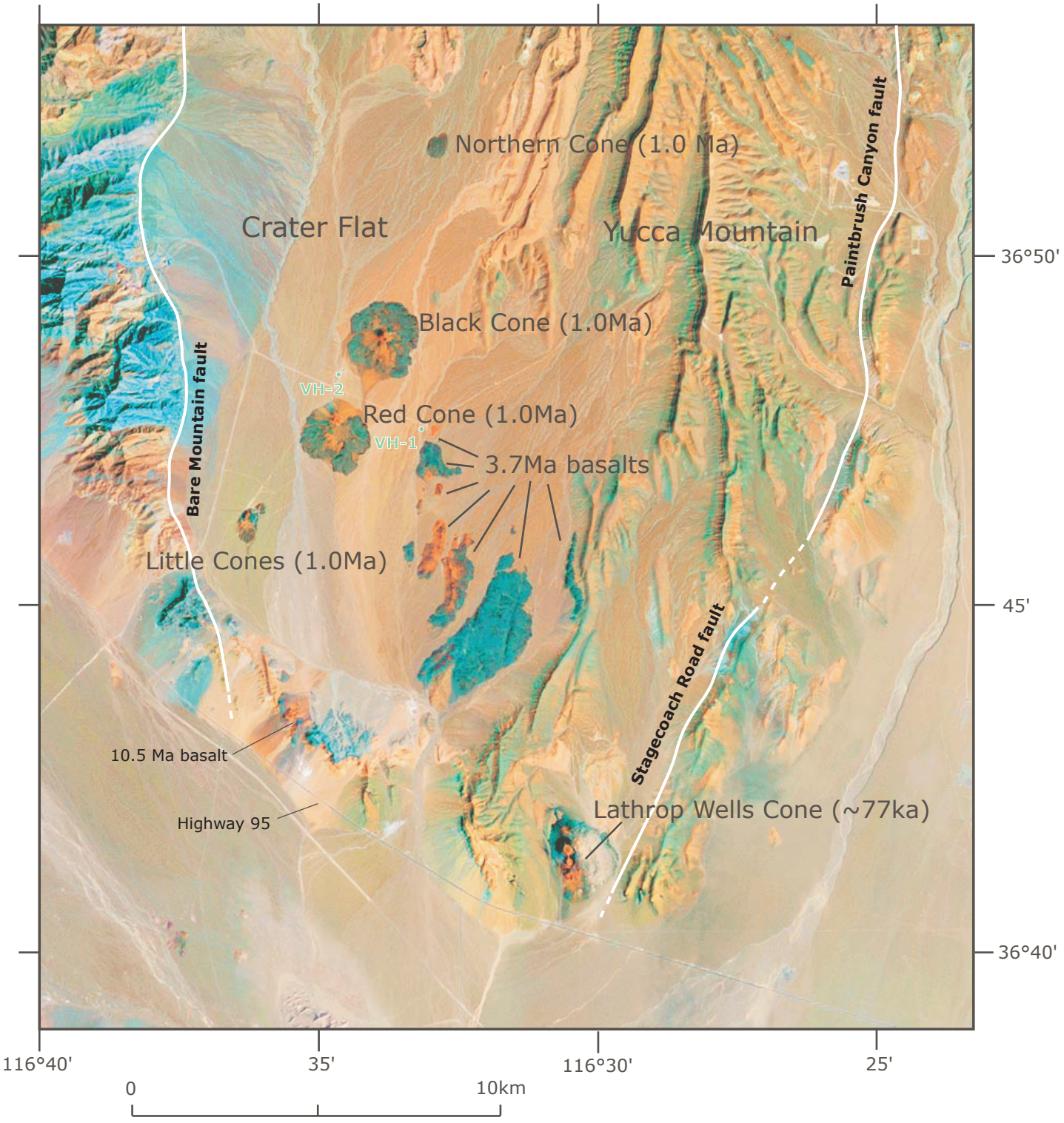

Figure 2. Ages and locations of basaltic volcanic centers near Yucca Mountain. Main faults that bound Crater Flat basin (Bare Mountain fault, Paintbrush Canyon -Stagecoach Road faults) shown in white.

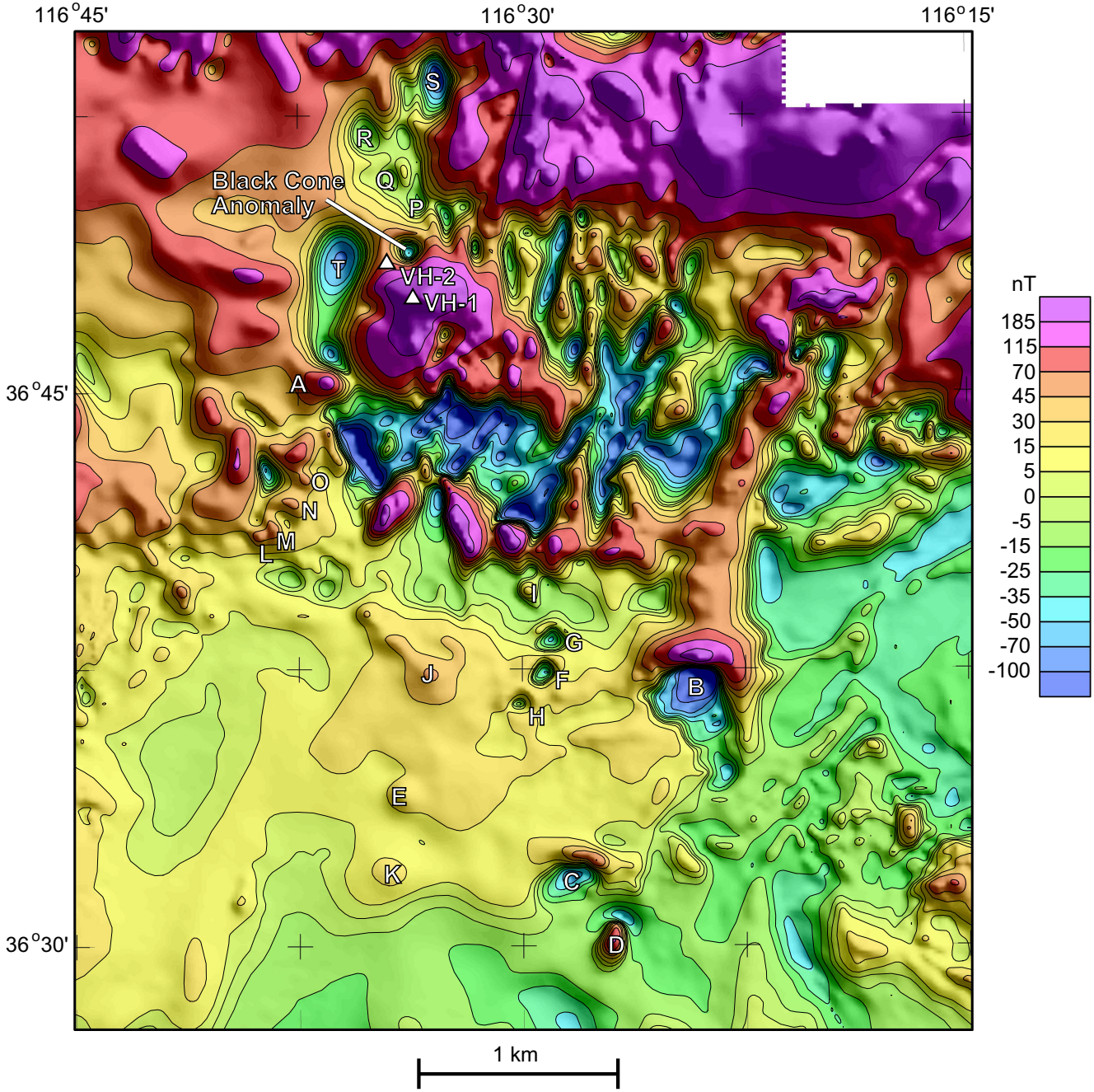

Figure 3. Magnetic anomalies, Crater Flat basin and northern Amargosa Desert, Nevada. Colors represent measured magnetic field intensities relative to the International Geomagnetic Reference Field. Color contour intervals were chosen objectively in order to equalize areas covered by each interval. Letters identify anomalies discussed in text and listed in Table 1.

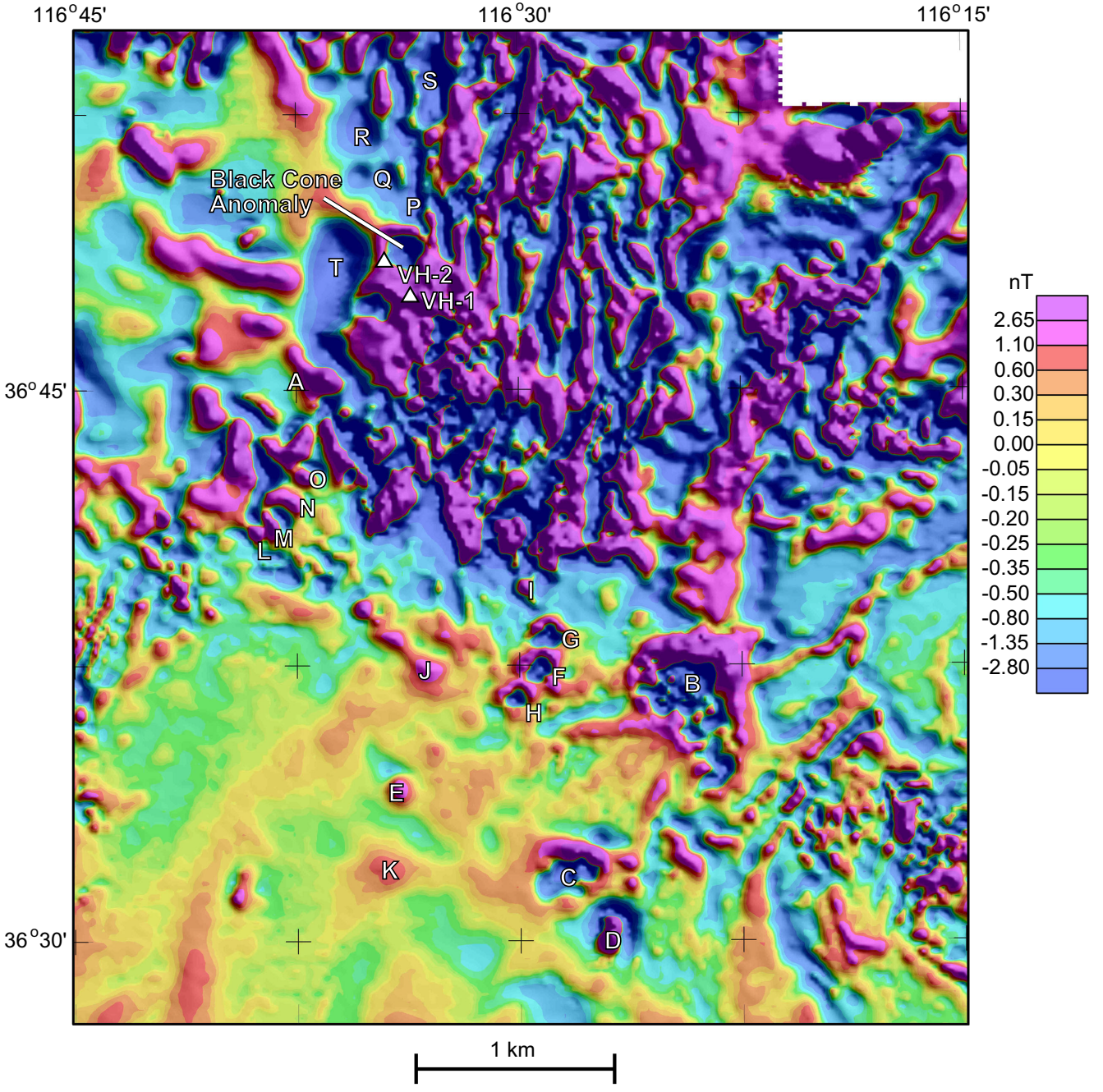

Figure 4. Residual magnetic anomalies, Crater Flat basin and northern Amargosa Desert, Nevada. Colors represent magnetic field intensity of residual magnetic anomalies, which were calculated by analytically continuing observed anomalies 50 m higher and subtracting from the original anomalies. See Figure 3 for additional explanation.

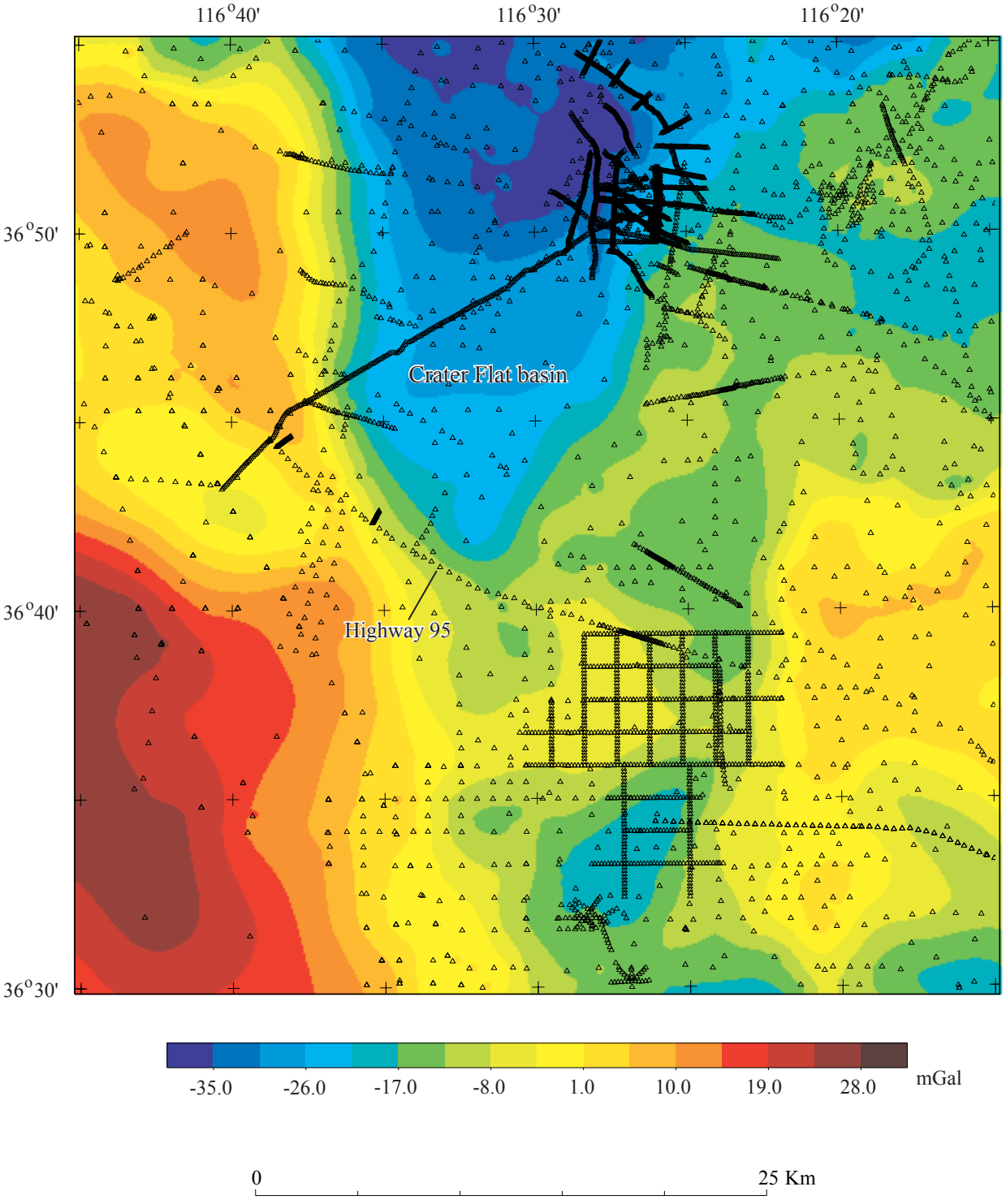

Figure 5. Isostatic residual gravity map of study area showing general shape and location of Crater Flat basin. Triangles represent gravity stations.

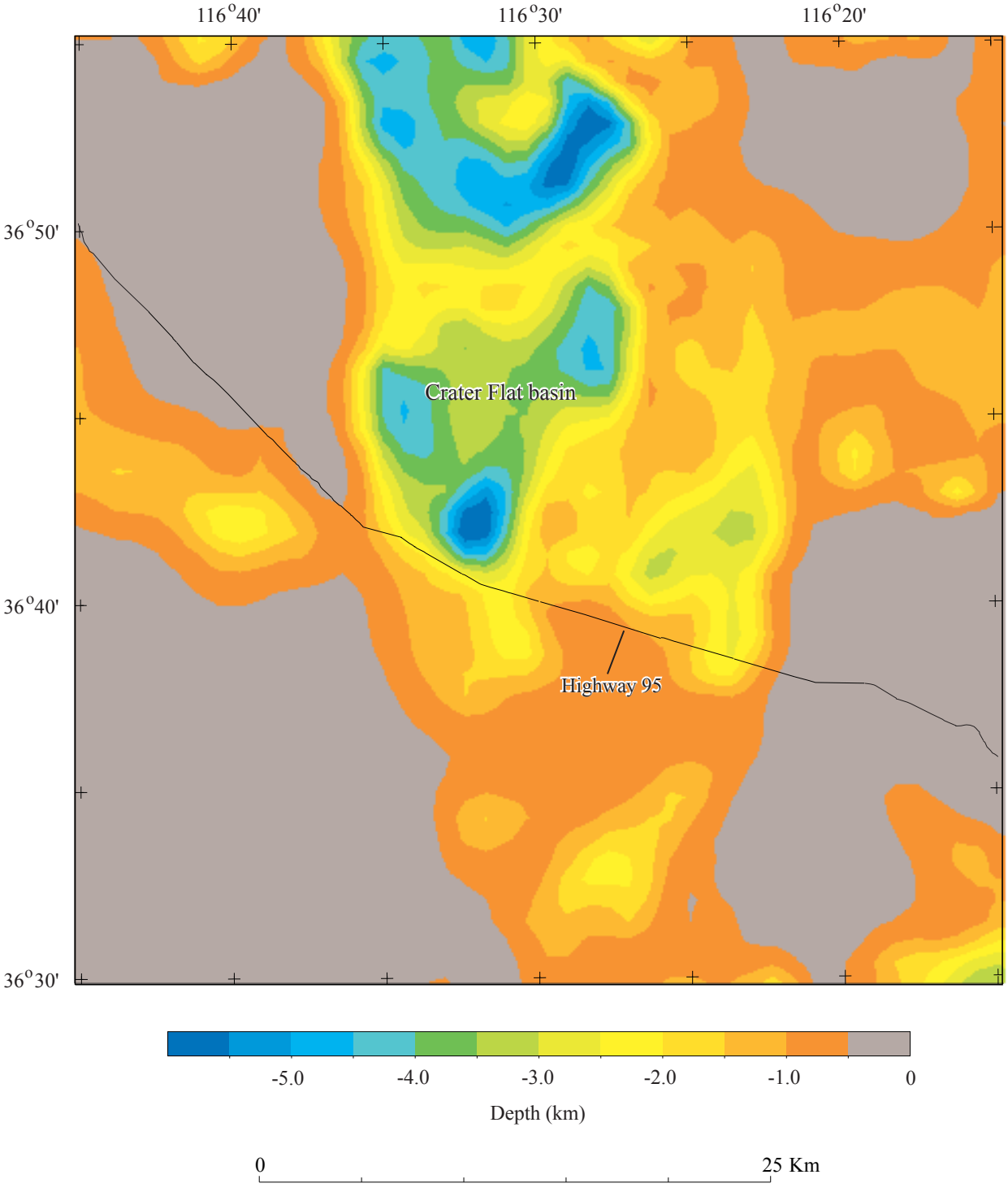

Figure 6. Estimated depth to basement (pre-Tertiary surface) in the study area based on the inversion of gravity data (from Hildenbrand and others, 1999).

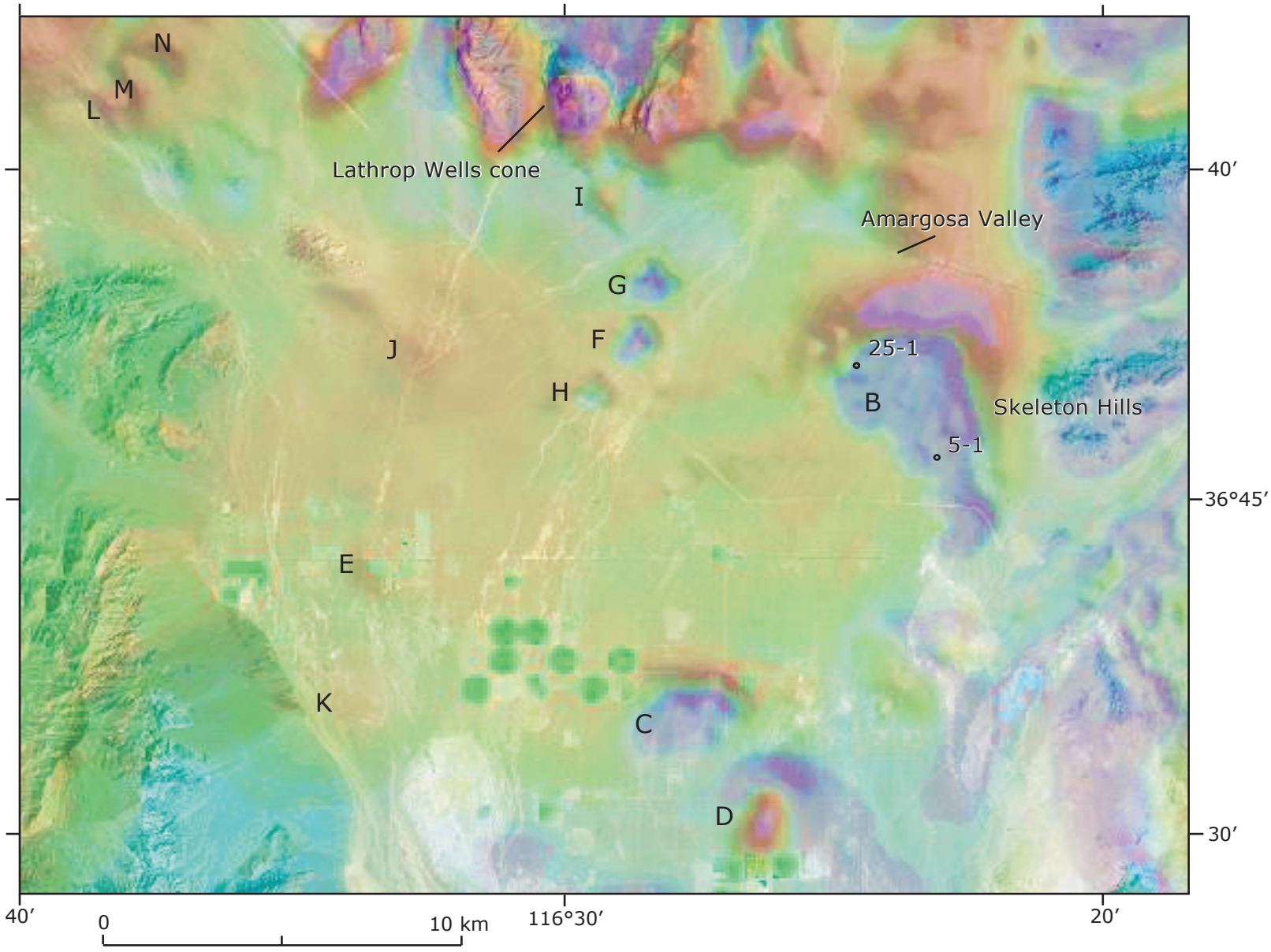

Figure 7. Labeled magnetic anomalies of possible Plio-Pleistocene basaltic origin (cf. fig. 3, Table 1). Landsat image overprint shows outcrops and drainage features of the northern Amargosa Desert. Locations of drill holes Felderhoff Federal 25-1 and 5-1 (Carr and others, 1995) shown in relation to anomaly B.

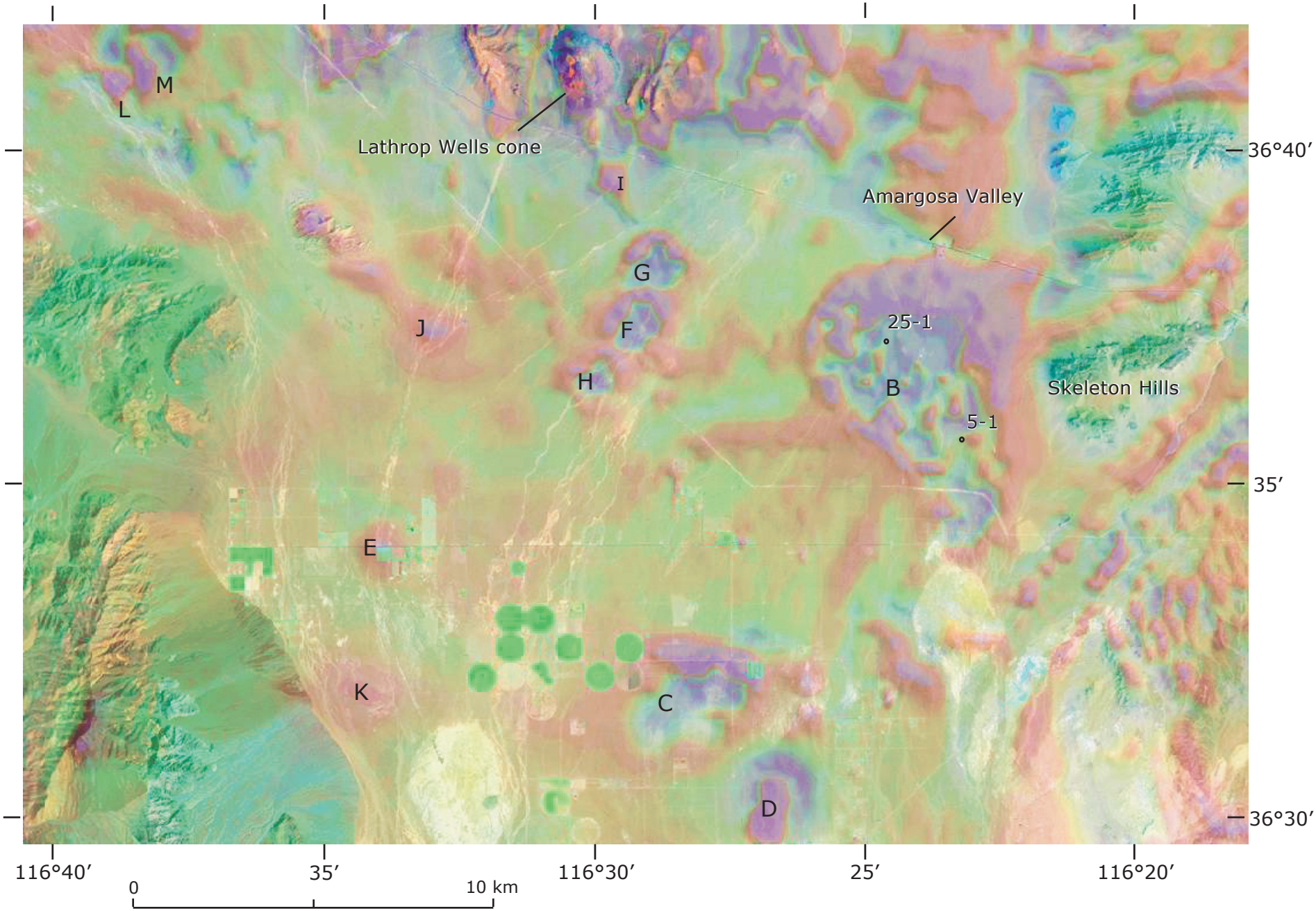

Figure 8. Labeled residual magnetic anomalies of possible Plio-Pleistocene basaltic origin (cf. fig. 3, Table 1). Landsat image overprint shows outcrops and drainage features of the northern Amargosa Desert. Locations of drill holes Felderhoff Federal 25-1 and 5-1 (Carr and others, 1995) shown in relation to anomaly B.

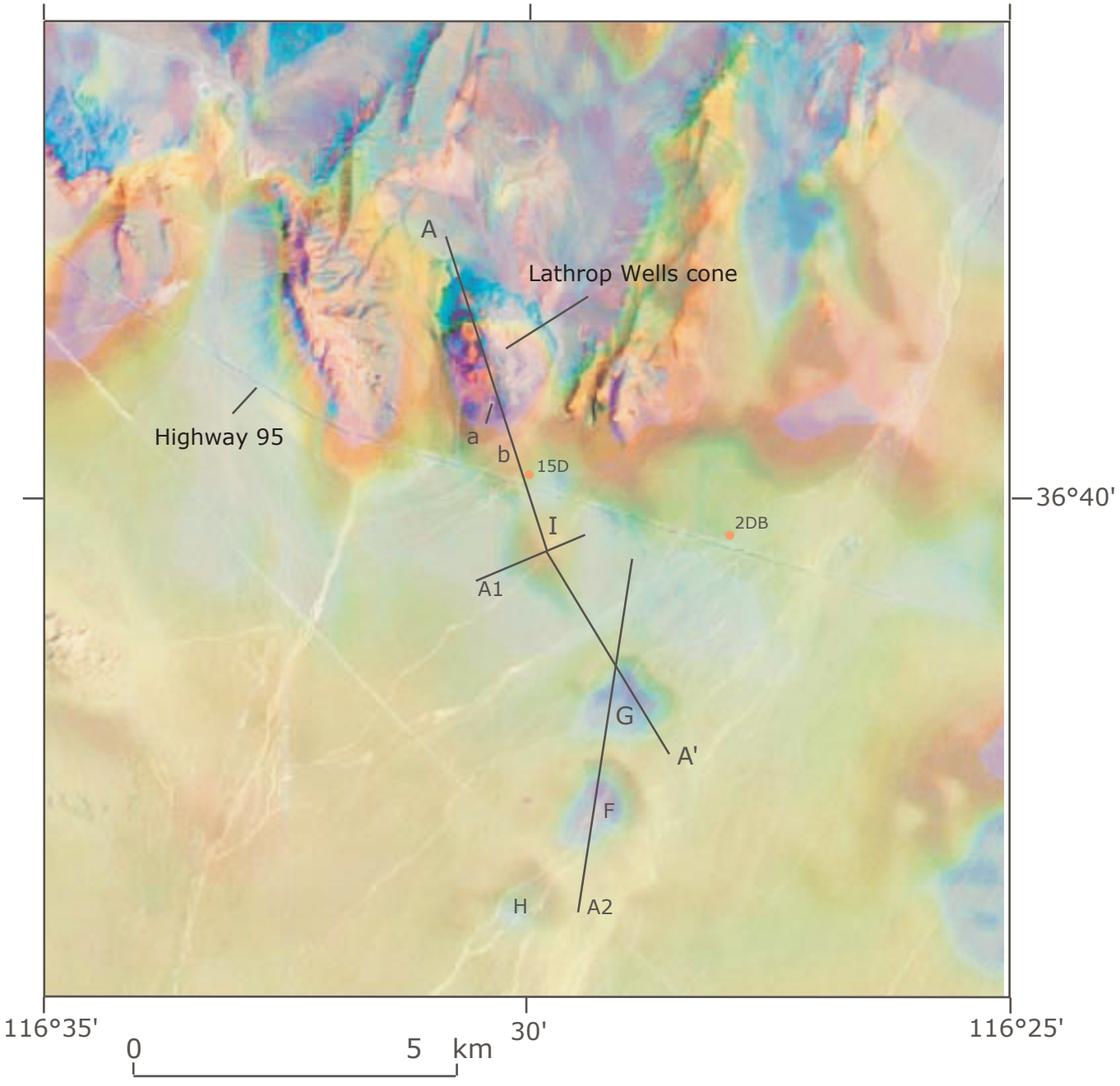

Figure 9. Magnetic anomaly map showing locations of transect AA' and profiles A1 and A2. Spectral feature 'a' indicates outcrop of Tiva Canyon Tuff, 'b' indicates a possible subsurface extension of Tiva Canyon Tuff. Labeled red dots show locations of Nye County boreholes NC-EWDP-15D and NC-EWDP-2DB.

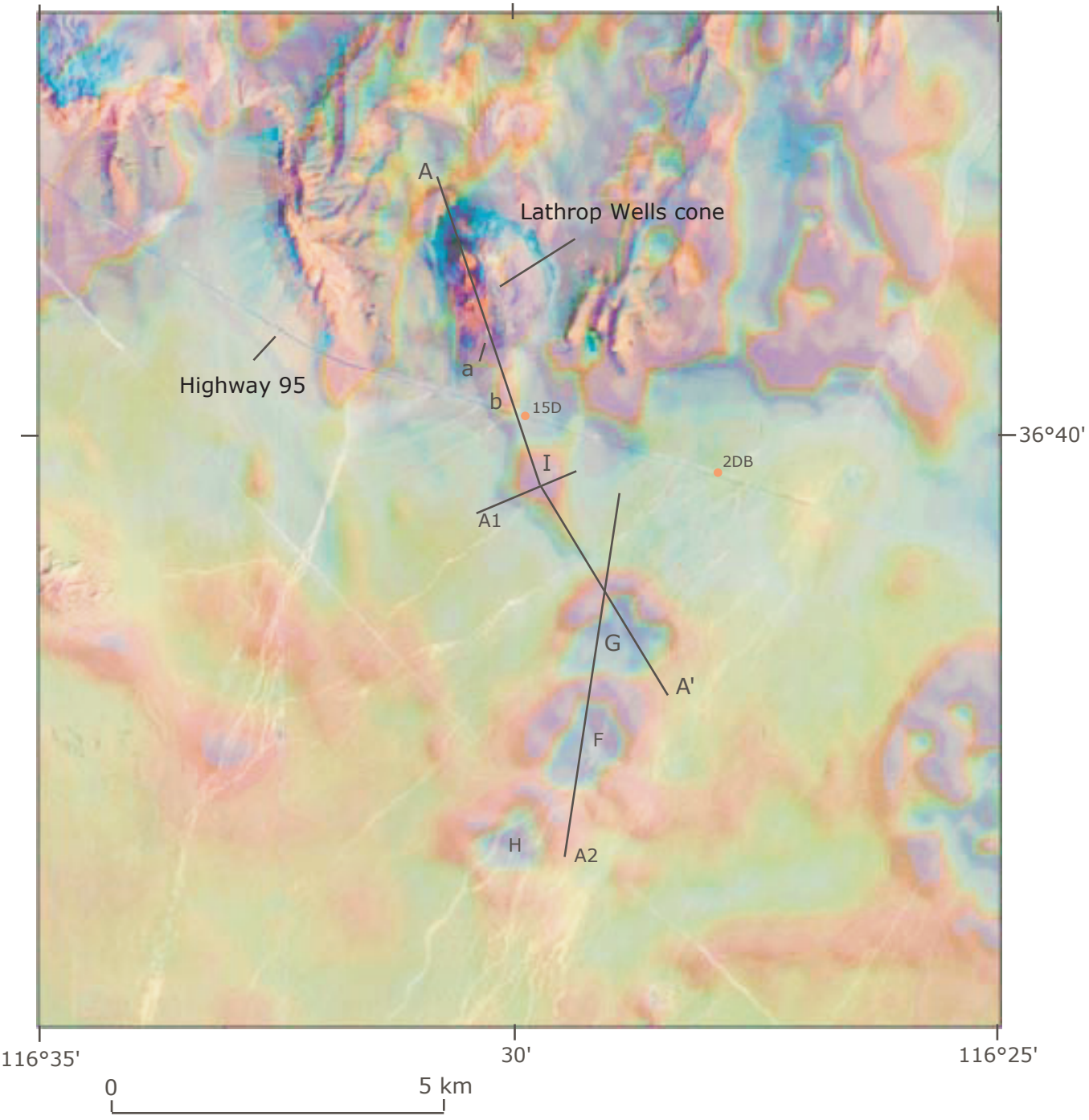

Figure 10. Residual magnetic anomaly map showing locations of transect AA' and profiles A1 and A2. See Figure 9 for additional explanation.

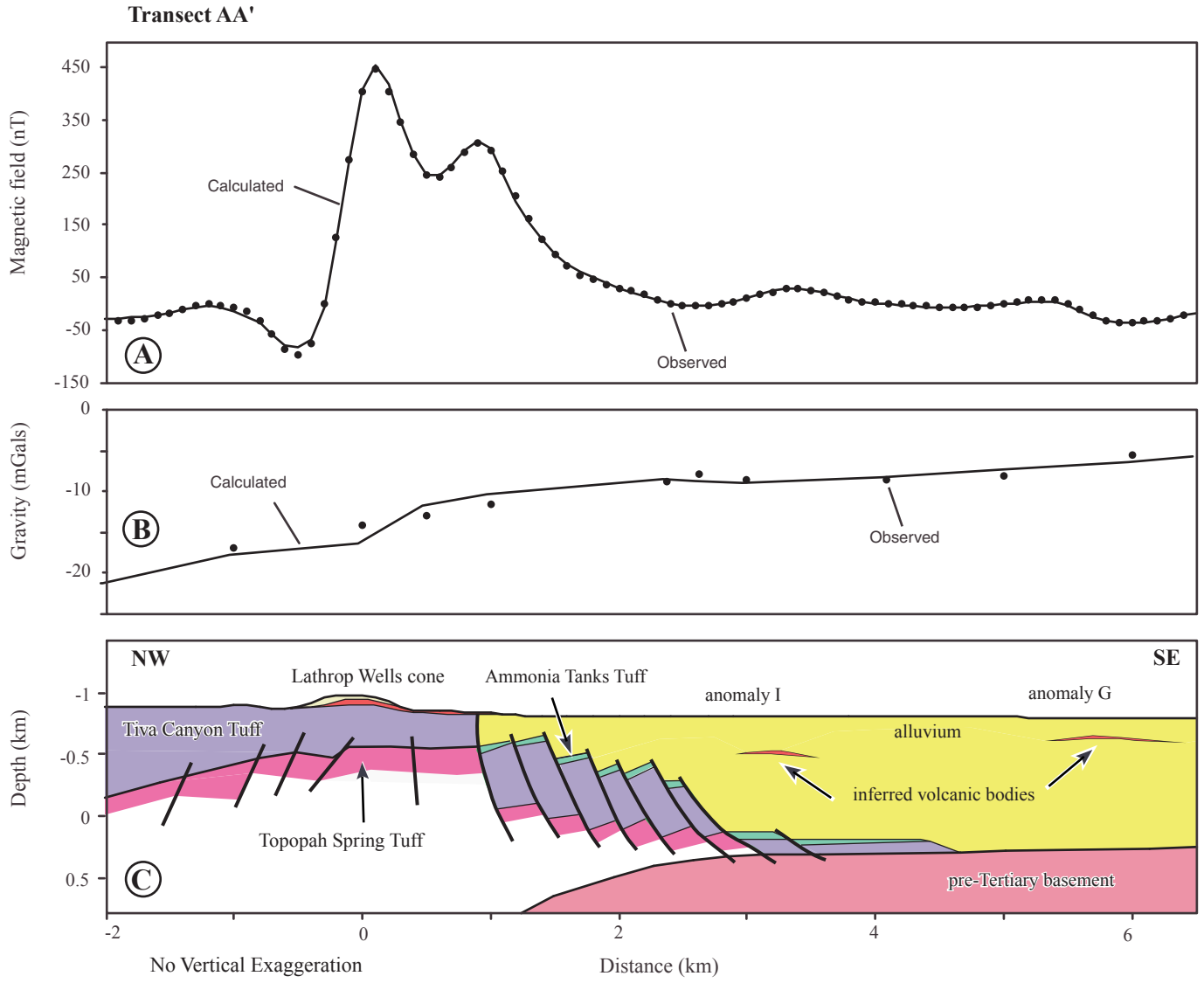

Figure 11. Geophysical model showing fits between observed and calculated (A) magnetic and (B) gravity profiles, and (C) a geologic interpretation of inferred subsurface structure along transect AA'. See figures 9 and 10 for location.

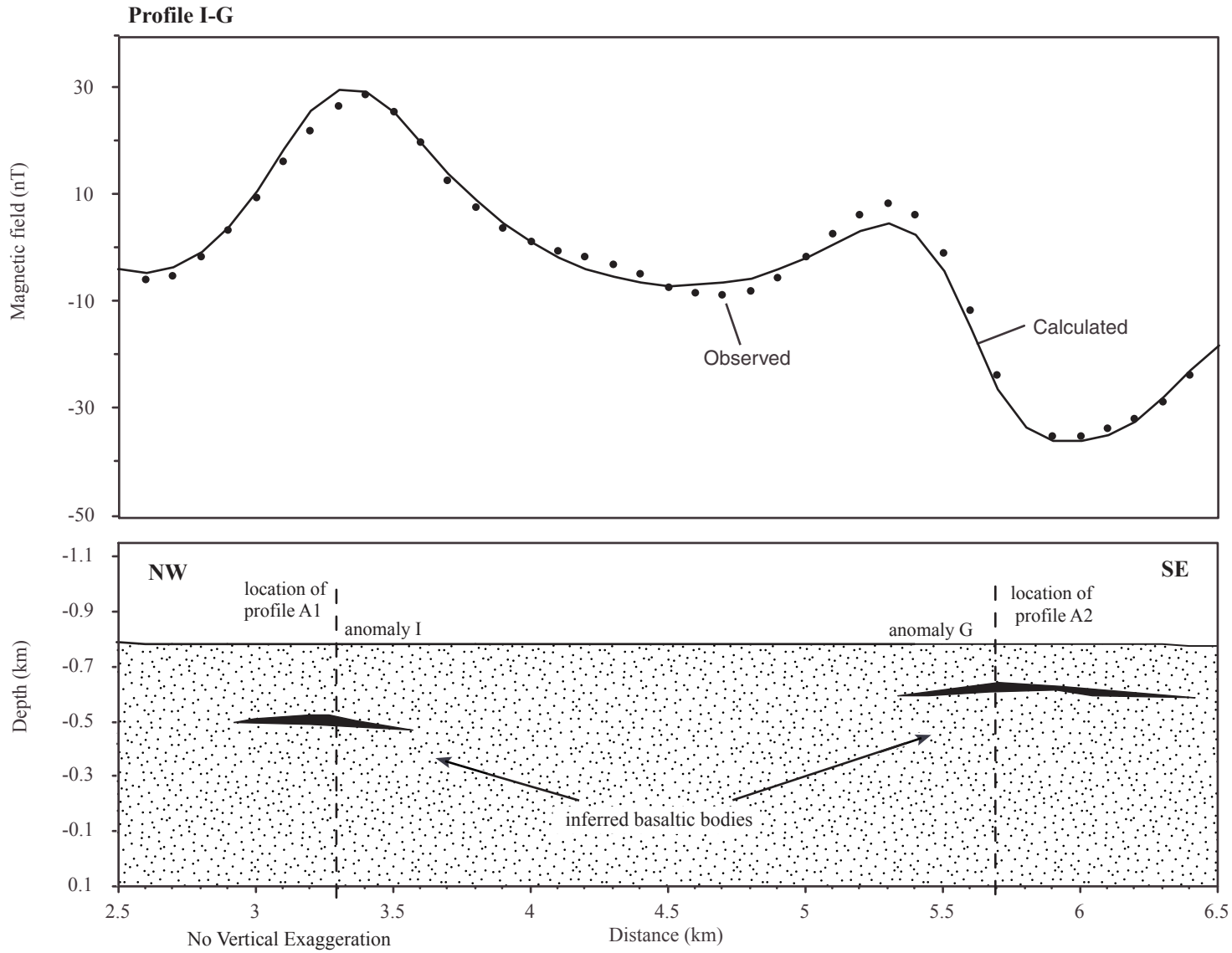

Figure 12. Sources for anomalies I and G along transect AA' modeled as buried basaltic bodies. See figures 9 and 10 for location.

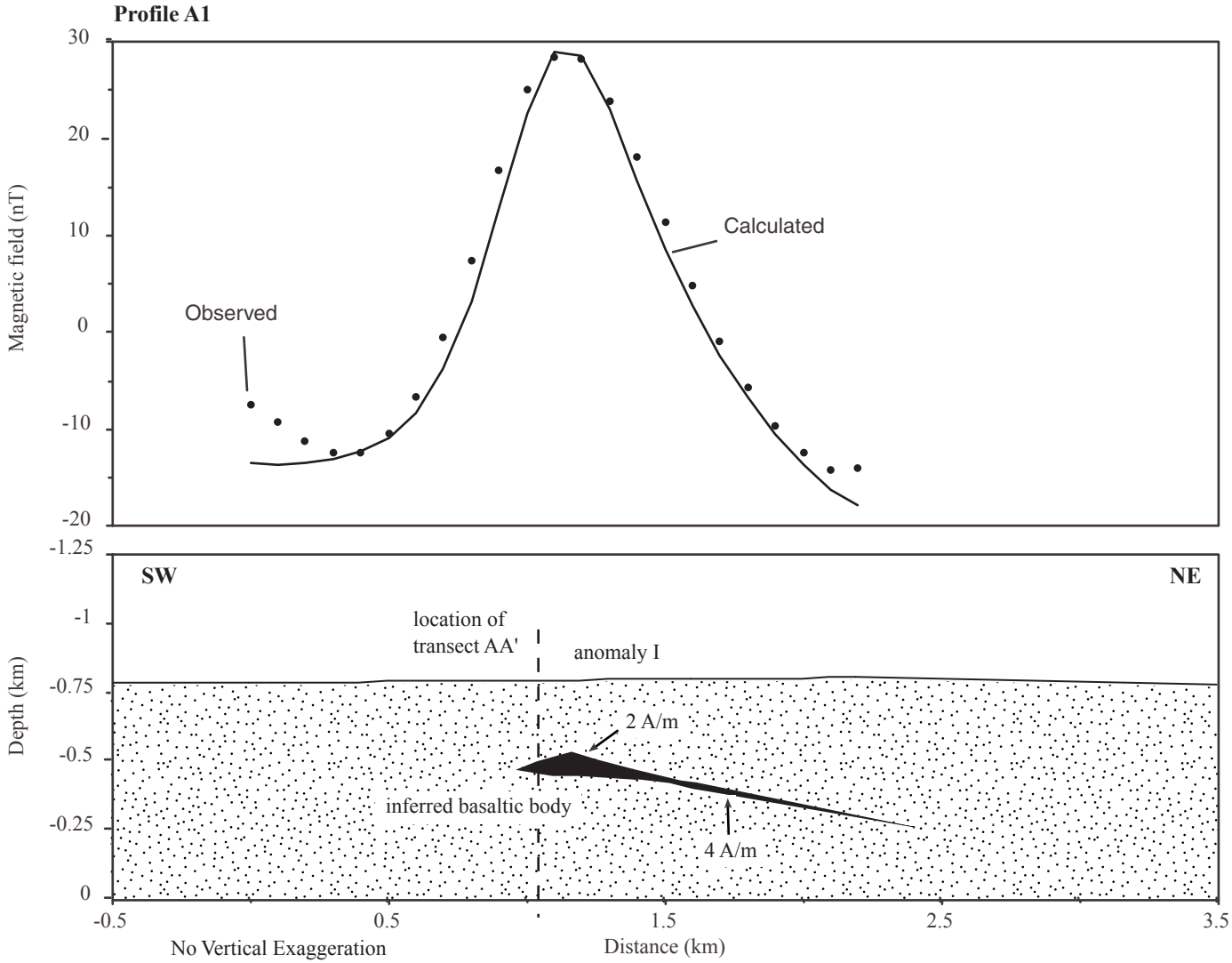

Figure 13. Source for anomaly I along profile A1 modeled as a buried basaltic body. See figures 9 and 10 for location.

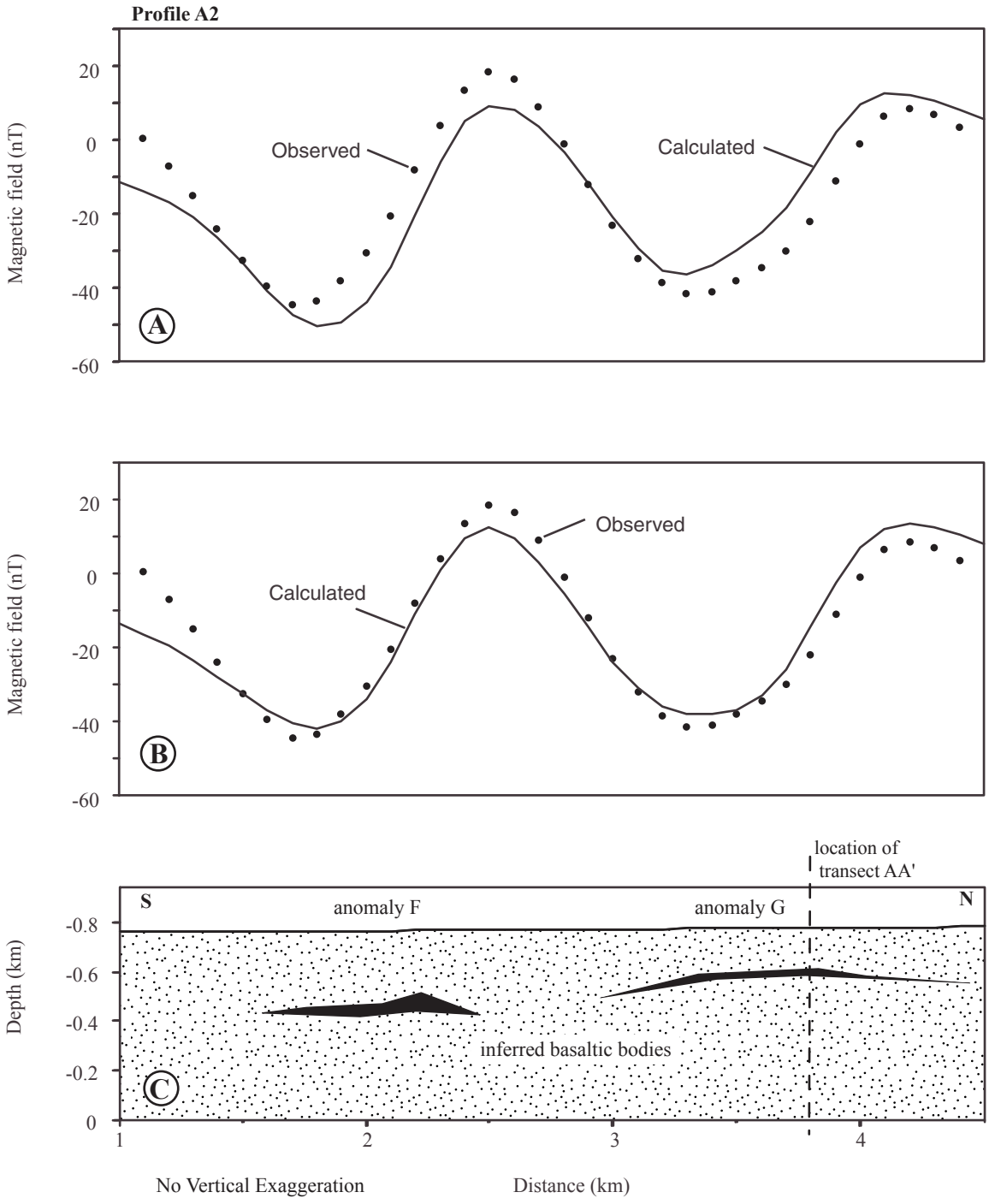

Figure 14. Sources for anomalies F and G along profile A2 modeled as buried basaltic bodies. See figures 9 and 10 for location. (A) Fit to observed magnetic field using assigned values for inclination and declination, and (B) fit assuming a different direction of magnetization for each body (see text).

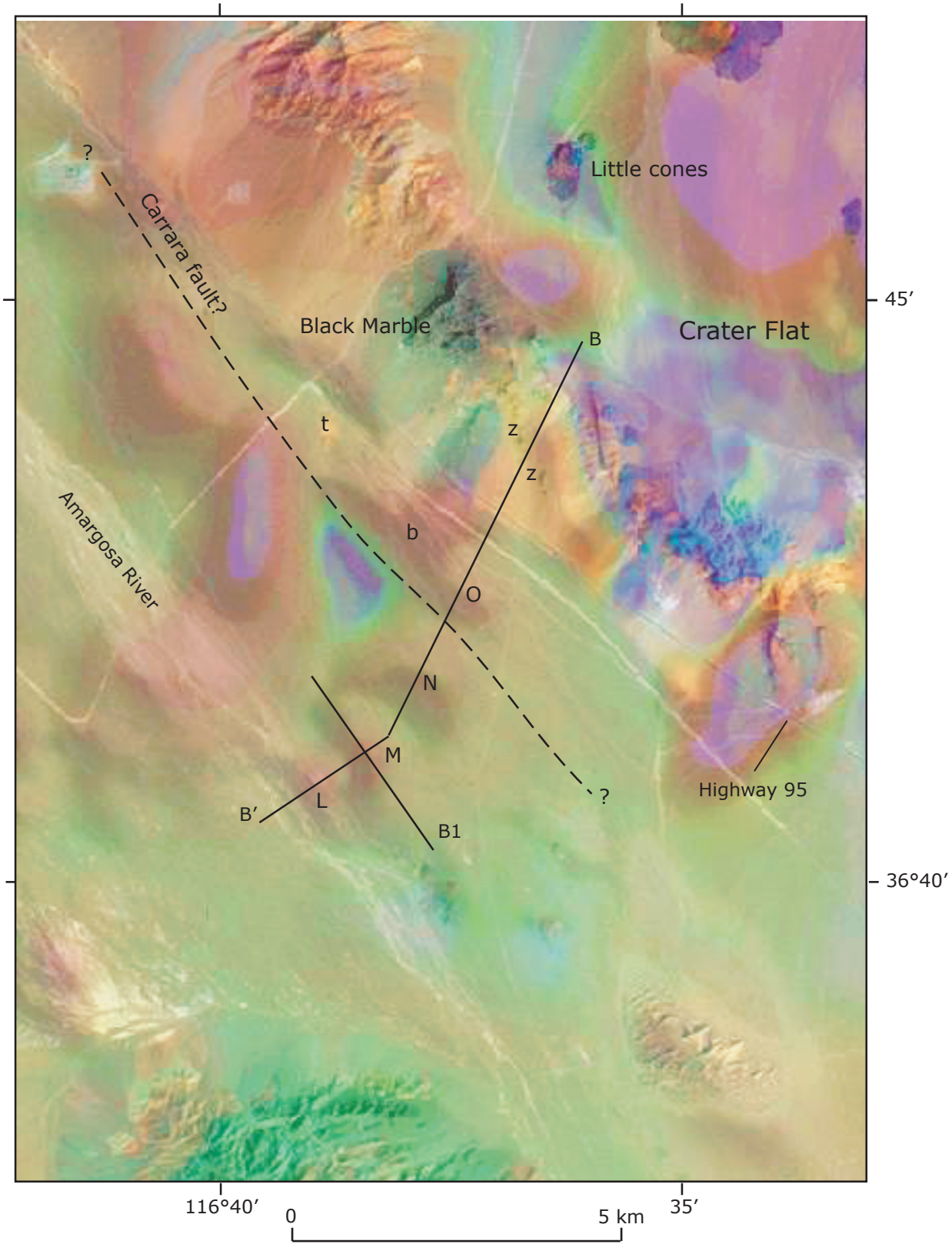

Figure 15. Magnetic anomaly map showing locations of transect BB' and profile B1. Transect BB' extends from near the Amargosa River into Crater Flat across anomalies L, M, N, and O. Lower case letters t and z represent outcrops relevant to the anomaly pattern and discussed in the text; letter b represents the inferred Carrara fault basalt of Connor and others (2000).

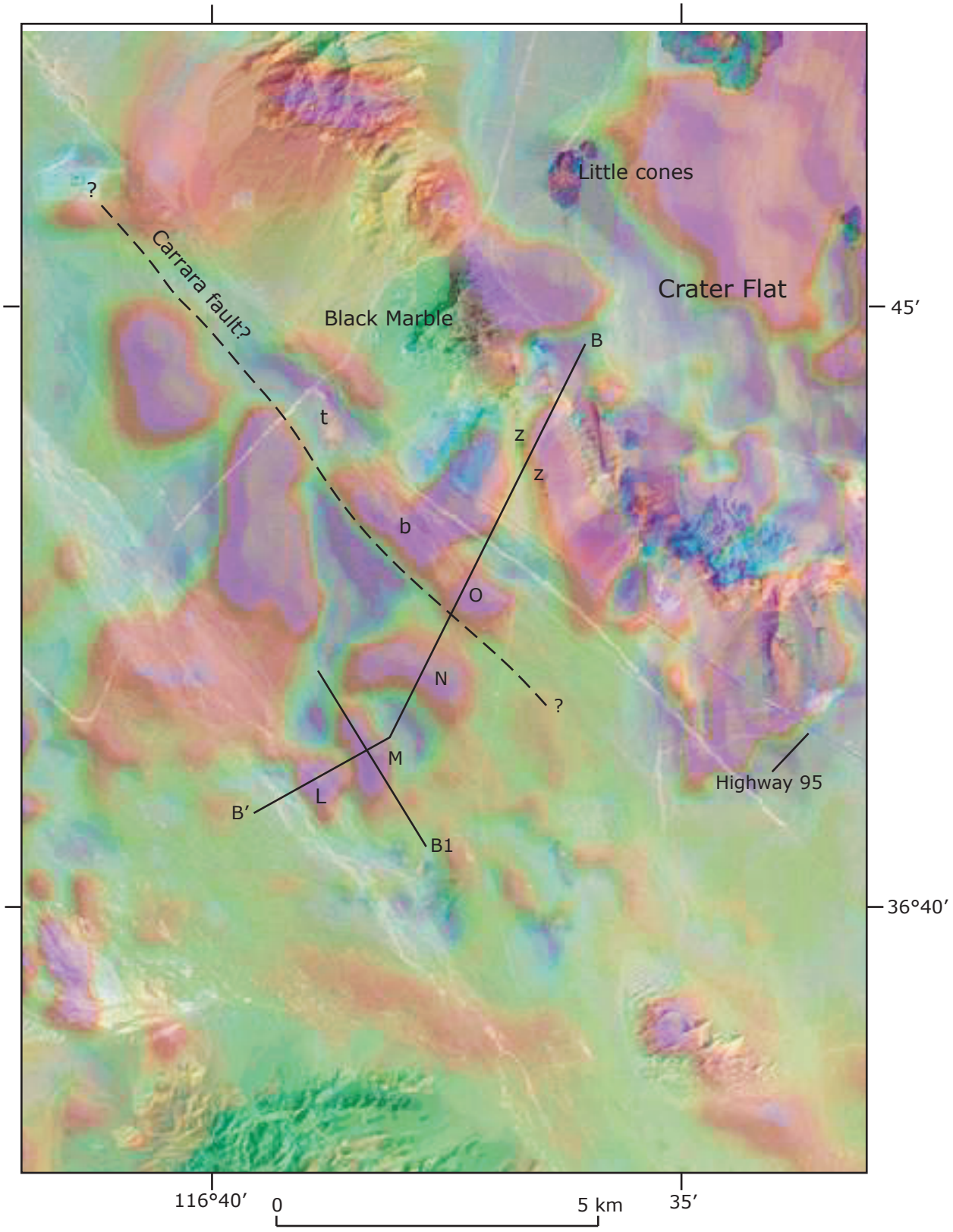

Figure 16. Residual magnetic anomaly map showing locations of transect BB' and profile B1. See Figure 15 for additional explanation.

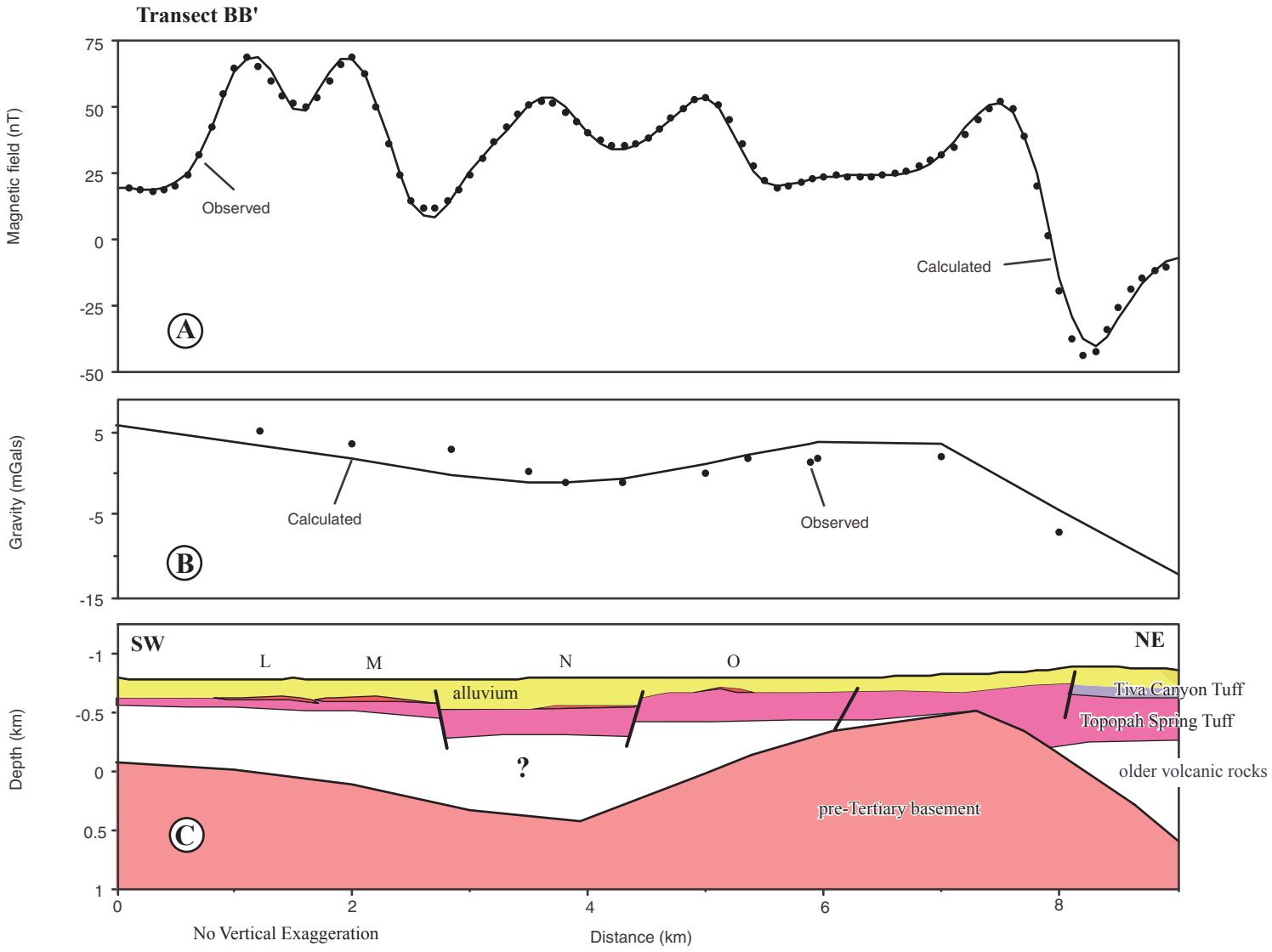

Figure 17. Geophysical model showing fits between observed and calculated (A) magnetic and (B) gravity profiles, and (C) a geologic interpretation of inferred subsurface structure along transect BB'. See figures 10 and 11 for location.

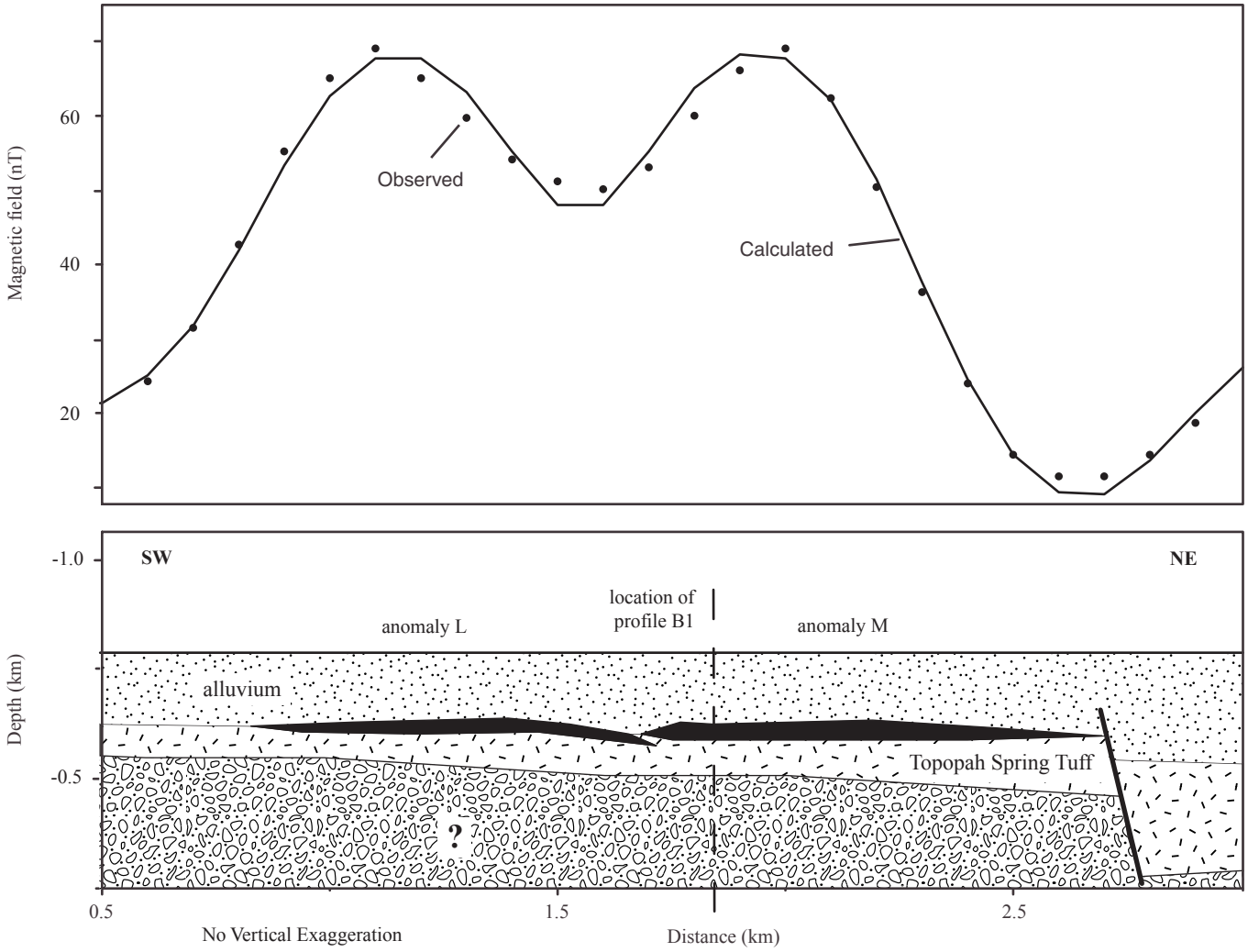

Figure 18. Sources for anomalies L and M along transect BB' modeled as buried basaltic bodies. See figures 15 and 16 for location.

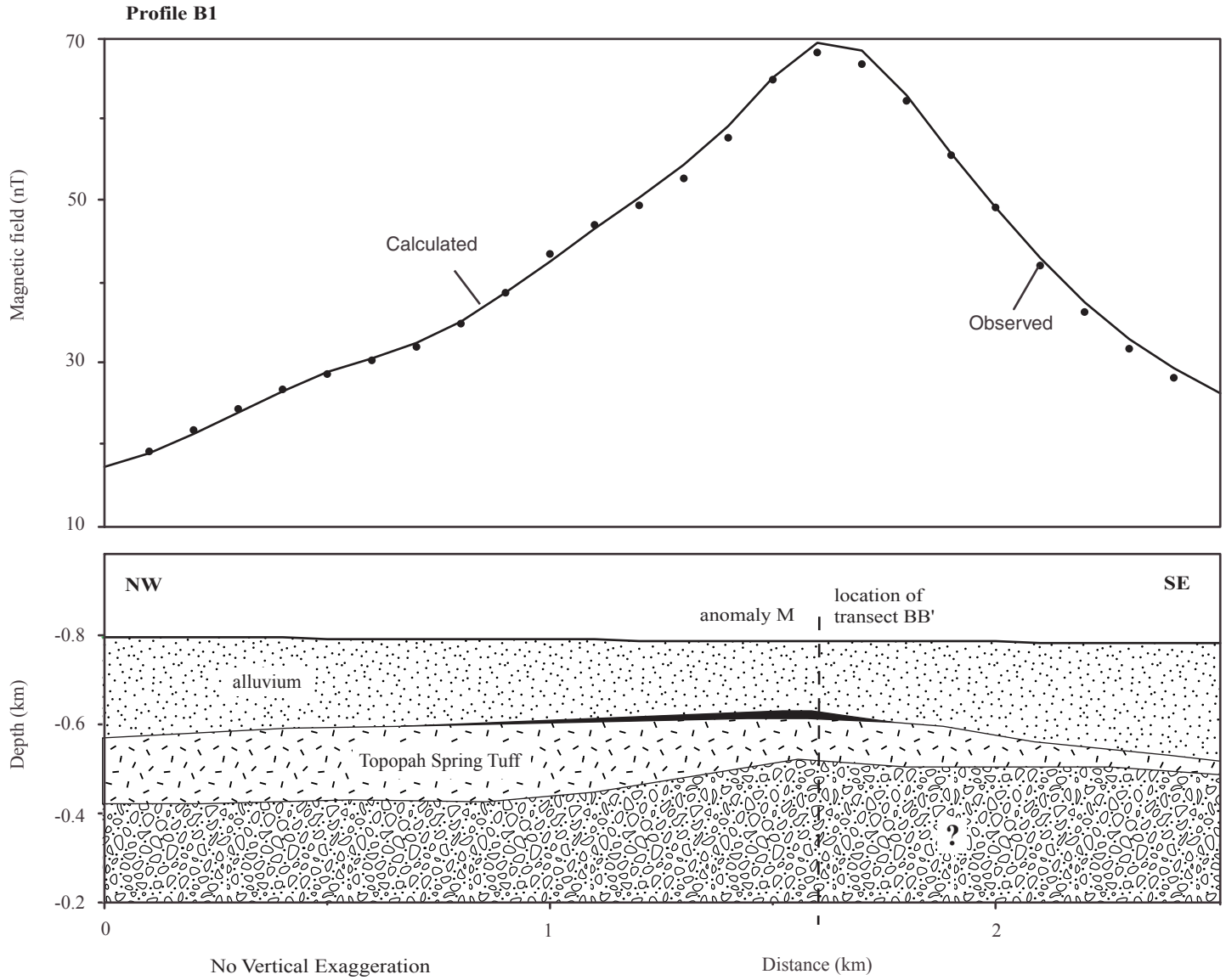

Figure 19. Source for anomaly M along profile B1 modeled as a buried basaltic body. See figures 15 and 16 for location.

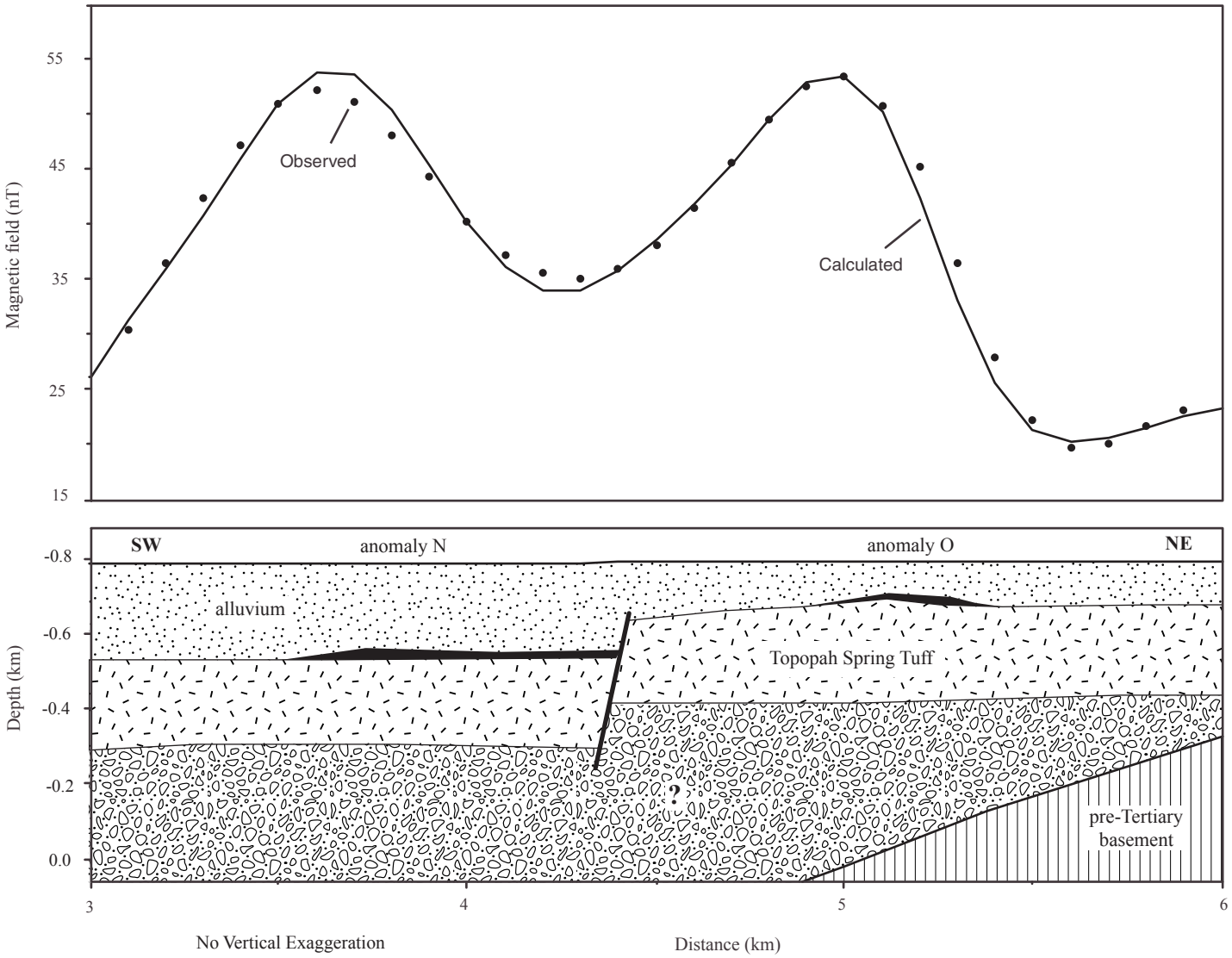

Figure 20. Sources for anomalies N and O along transect BB' modeled as buried basaltic bodies. See figures 15 and 16 for location.

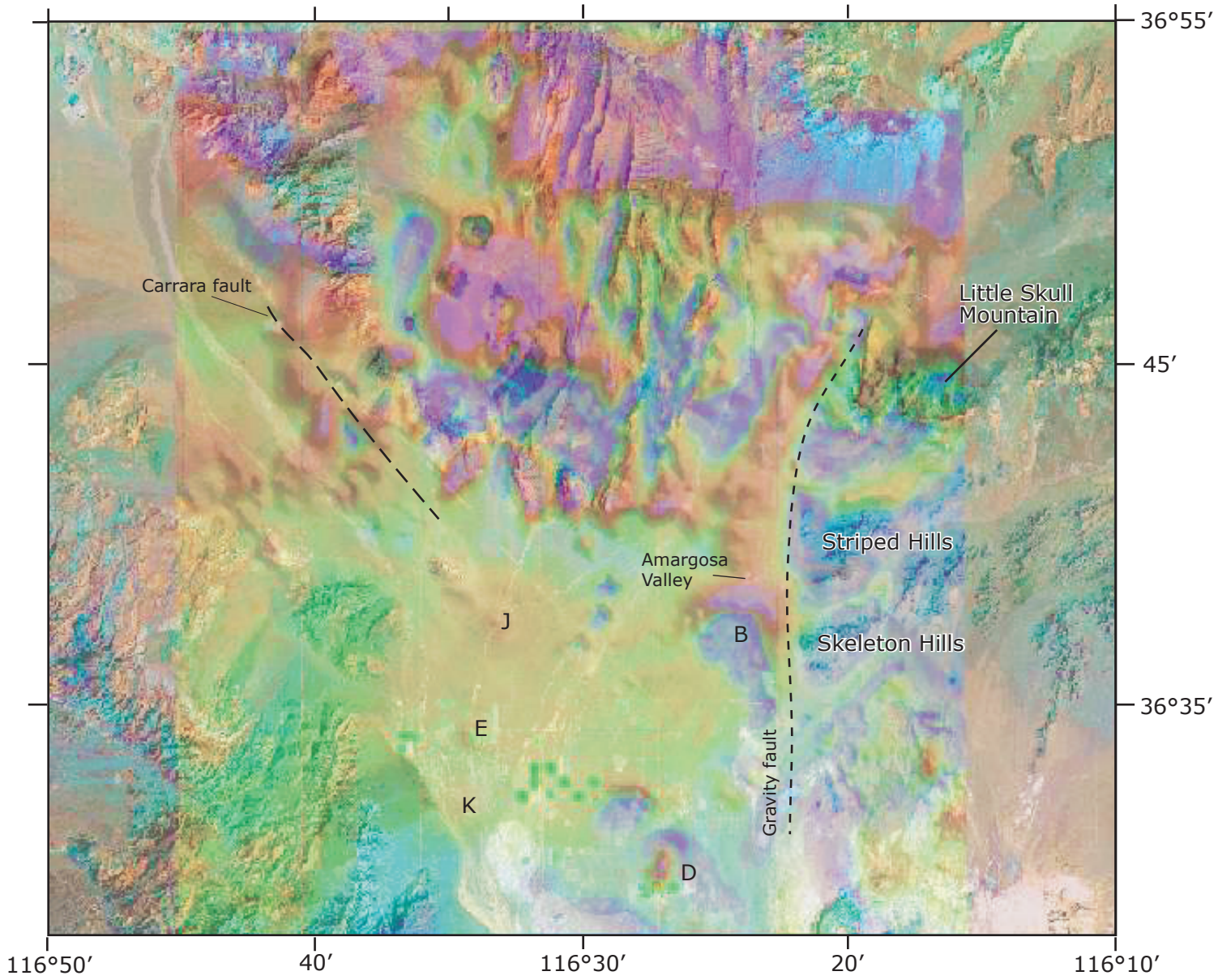

Figure 21. Aeromagnetic map and superposed Landsat image of outcrops and terrain features of the Yucca Mountain area.

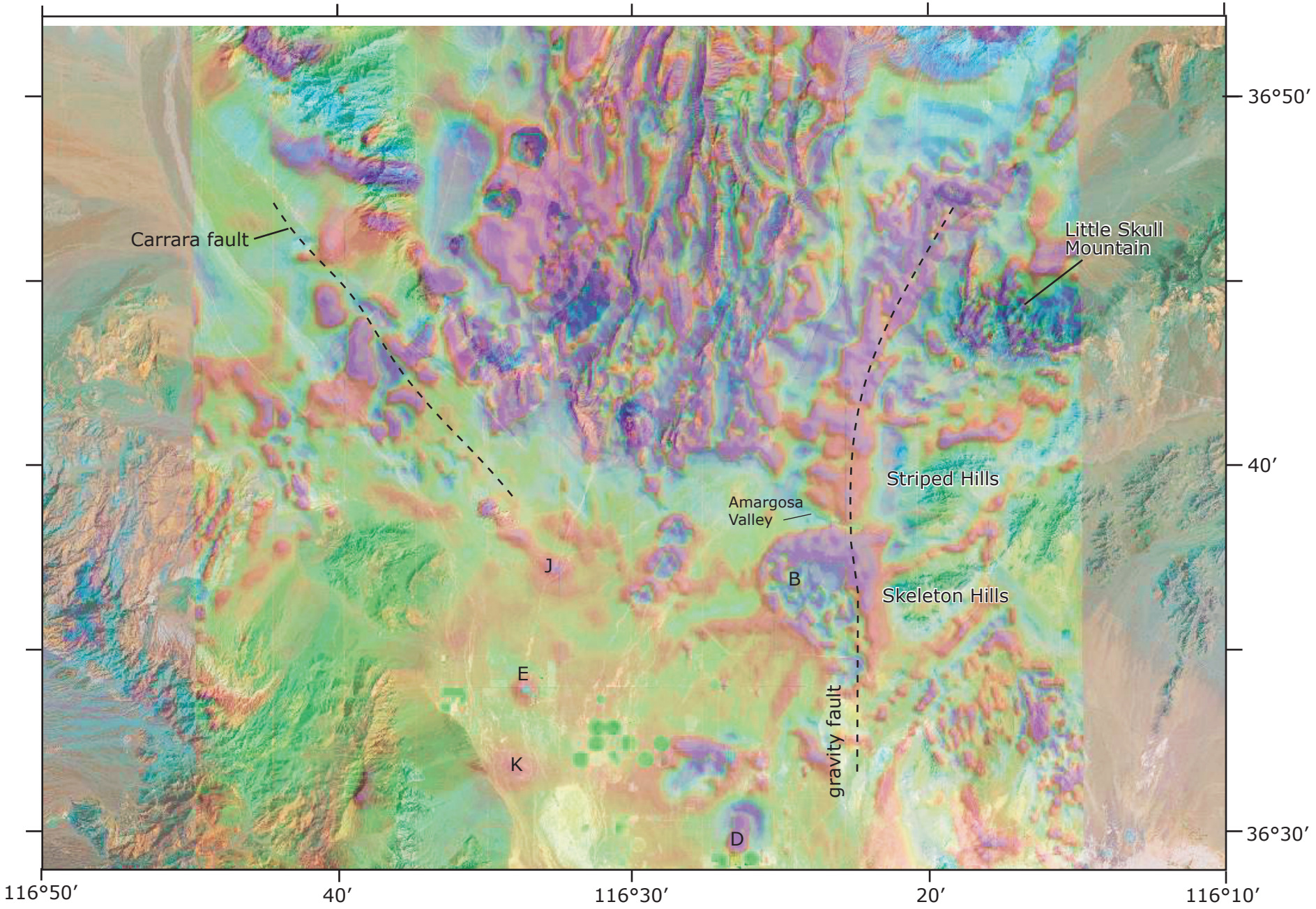

Figure 22. Residual aeromagnetic map and superposed Landsat image of outcrops and terrain features of theYucca Mountain area.

Table 1. Tabulated labels and features of the magnetic anomalies thought to represent buried volcanic centers in Crater Flat and Amargosa Desert area, Nevada. Anomaly label numbers indicate sources: 1: this report; 2: PVHA, 3: Connor and others, 2000, 4: Langenheim, 1995. Column labeled rank indicates authors' confidence that anomalies have basalt sources: conf: confirmed, 1: high confidence, 2: probable, 3: equivocal, 4: low confidence.

Rank	Anomaly label 1	2	3	4	Location (lat-lon coords N, W)	Polarization	Amplitude, nT (ground level)	Depth to top, m	Anomaly/body characteristics
1	A	A	A	F	36° 45.27' 116° 36.48'	+	~1000	~206 (Langenheim, 1995)	Extends NW, has double peak
conf.	B	B	AAB	B	36° 36.7' 116° 24.14'	-	912 and -1247	~150 (Langenheim and others, 1993); 73 (Carr and others, 1995)	~77m thick (Carr and others, 1995)
1	C	C	AAC	C	36° 31.82' 116° 28.27'	-	600	~200 (Langenheim, 1995)	
1	D	D	AAD	D	36° 30.02' 116° 26.94'	+	850	~175 (Langenheim, 1995)	
2	E	E	AAE	E	36° 34.06' 116° 34.03'	+			
1	F	F	AAA		36° 37.36' 116° 29.20'	-	70-150	~250	F, G, H form NE alignment
1	G	G	AAA		36° 38.23' 116° 29.00'	-	70-150	~150	
1	H				36° 36.56' 116° 30.06'	-	70-150		
2	I				36° 39.52' 116° 29.78'	+		~250	
3	J				36° 37.32' 116° 33.15'	+			
3	K				36° 31.97' 116° 34.50'	+			
3	L				36° 41.09' 116° 38.87'	+		~150	L, M, N, O form NE alignment
3	M				36° 41.26' 116° 38.27'	+		~150	
3	N				36° 41.98' 116° 37.71'	+		~220	
3	O				36° 42.60' 116° 37.24'	+		~50	
4	P				36° 50.22' 116° 33.41'	-			
4	Q		C		36° 50.76' 116° 34.31'	-			
4	R				36° 51.98' 116° 35.16'	-			
4	S				36° 53.43' 116° 32.81'	-			